2.4.1 Plume mixing and behaviour

The brine discharged via the diffuser is denser than the receiving waters because of its higher salinity. As a result, and noting the vertical angle of the discharge, on release the effluent initially rises to a point where buoyancy forces become dominant and a descending trajectory commences until the plume eventually reaches the seabed. The highest point in the plume trajectory is referred to as the terminal rise height and the point where it reaches the seabed is termed the impact point (Figure 2-21). The region where this process takes place is denoted the nearfield (Roberts and Abessi 2014). In the nearfield, mixing processes are influenced by the combination of the discharge jet momentum in the ascending phase, and by buoyancy and the associated shear-induced entrainment in the descending phase. Whilst the nearfield region size is influenced by the characteristics of the discharge and ambient current conditions, it generally confined to within tens of meters of the diffuser.

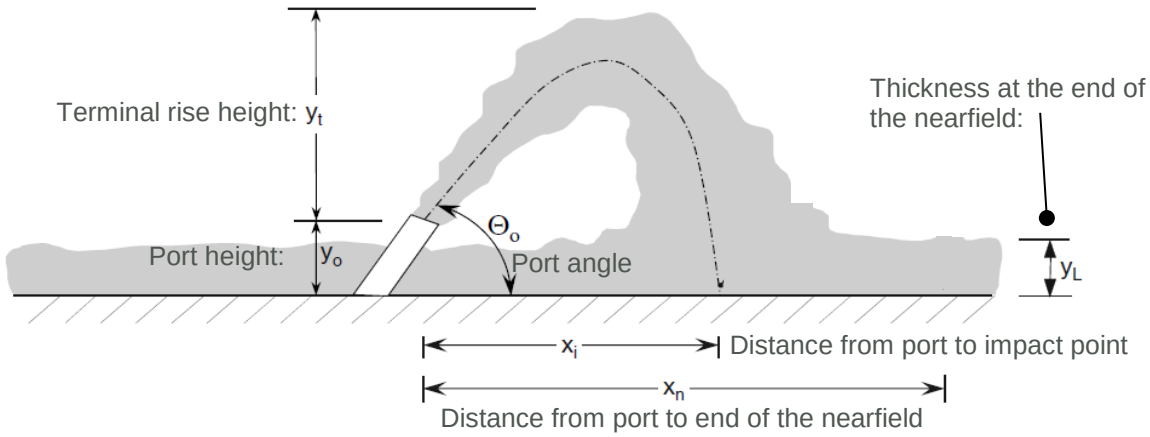

Figure 2-21 Definition diagram for nearfield characteristics (adapted from Roberts et al. 1997)

As the plume moves away from the point of the discharge, the initial jet momentum and buoyancy become less relevant for the mixing and trajectory of the discharged water, and the ambient conditions start to dominate. In this region, transport and mixing processes are controlled by the combination of shear mixing, bottom friction and local currents. This region where ambient processes dominate is termed farfield. The farfield is generally of the order of hundreds of metres away from common seawater desalination discharges.

In between the near and farfield, there is transition zone generally classified as the midfield, which is commonly where regulatory mixing zones are applied. CWR (2007a,b) conducted a series of field experiments near the PSDP diffuser, with emphasis in the transition from the nearfield to the farfield. CWR (2007a) found the discharge at near full flow (2.19 m^3/s) reached a maximum height of 9.0 m from seabed and dilutions above 50 at 20.0 m or more away either side of the diffuser (CWR 2007a, Figure 2-22).

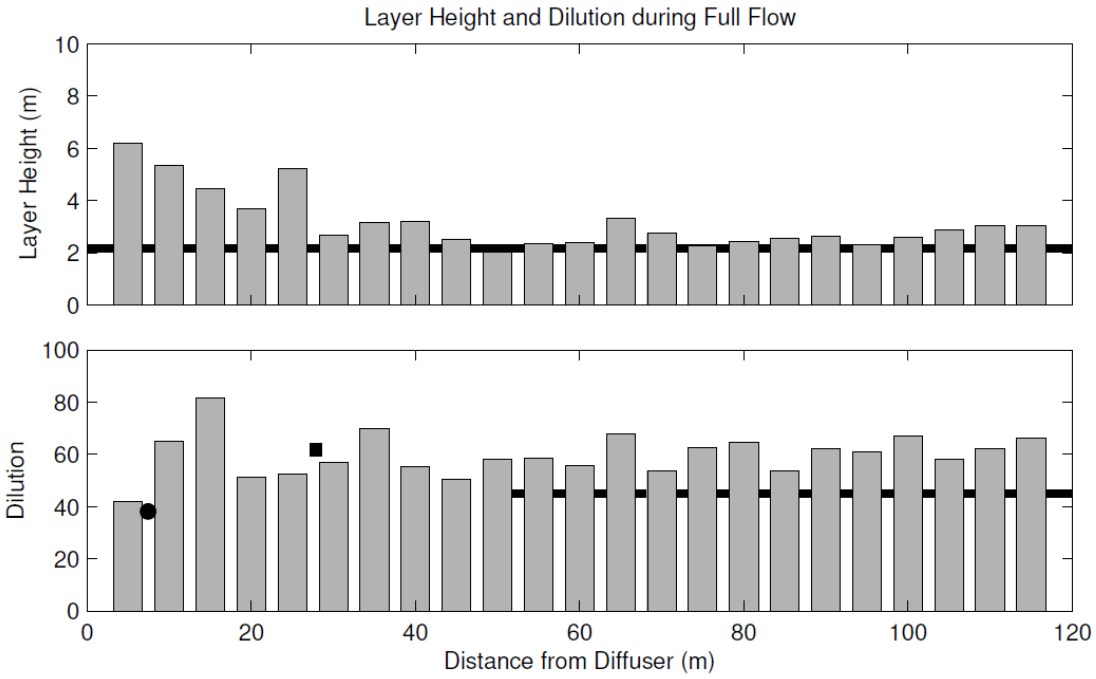

Figure 2-22 Ensemble average of saline discharge layer height (top panel) and dilution (bottom panel) for bins corresponding to 5 m intervals away from diffuser for full flow. Horizontal line in background of top panel show theoretical layer thickness from Roberts et al. (1997). Symbols in bottom panel show location and dilution at impact point (circle) and edge of mixing zone (square) predicted by Roberts et al. (1997). The horizontal line on the bottom panel represents the design target dilution of 45 times (marked from 50 metres from the diffuser onwards). (reproduced from CWR 2007a)

As the discharge moved away from the diffuser, CWR (2007b) reported that it travelled down the seabed slope towards Calista Channel where it was then transported towards Stirling Channel (Figure 2-23) until it eventually made its way to the deep basin of the Sound (Figure 2-24). Whilst in the channel, the plume thickness was between 5.0 and 3.0 m and reduced as it moved towards the Sound deep basin (Figure 2-23 and Figure 2-24). By the time it reached the edge of the deep basin of the Sound its thickness quickly reduced to less than 1.0 m and it was then not discernible from about 1.0 km away from Stirling Channel exit location (a difference of less than 0.2 salinity units to the overlying water - Figure 2-24, CWR 2007b).

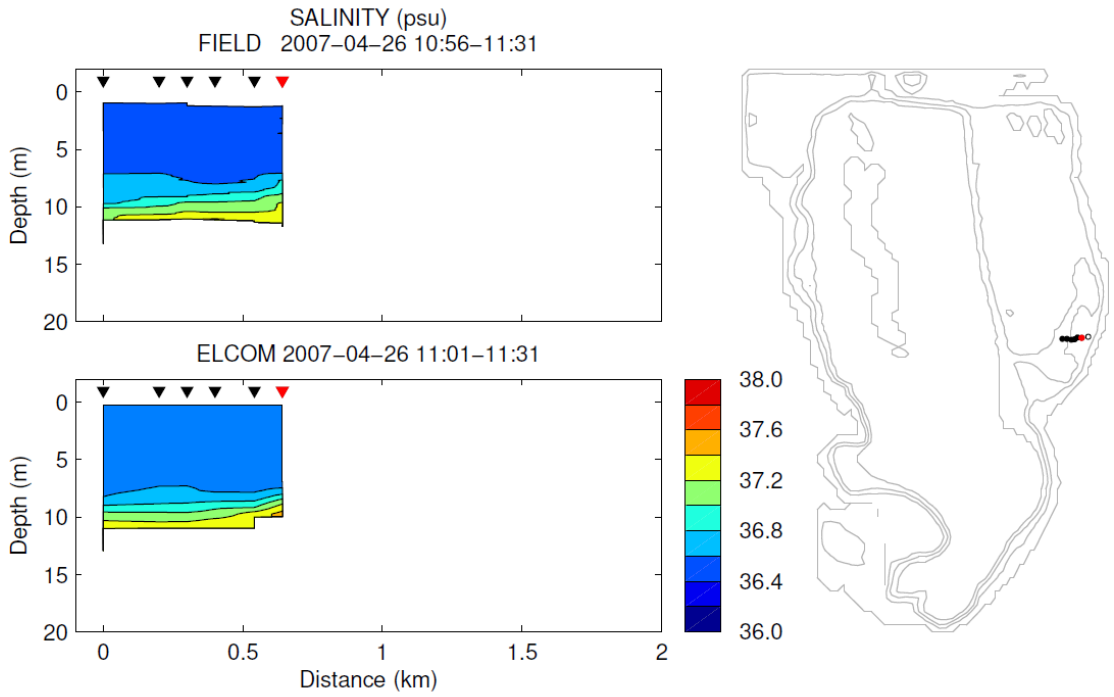

Figure 2-23 Measured (upper panel) and simulated (lower panel) salinity along a transect from the diffuser to the main shipping channel following the dye release in the morning of 26 Apr 2007. Locations of transect profiles are shown on the map to the right of each panel; map has diffuser marked; red symbols indicate profile closest to diffuser. (Reproduced from CWR 2007).

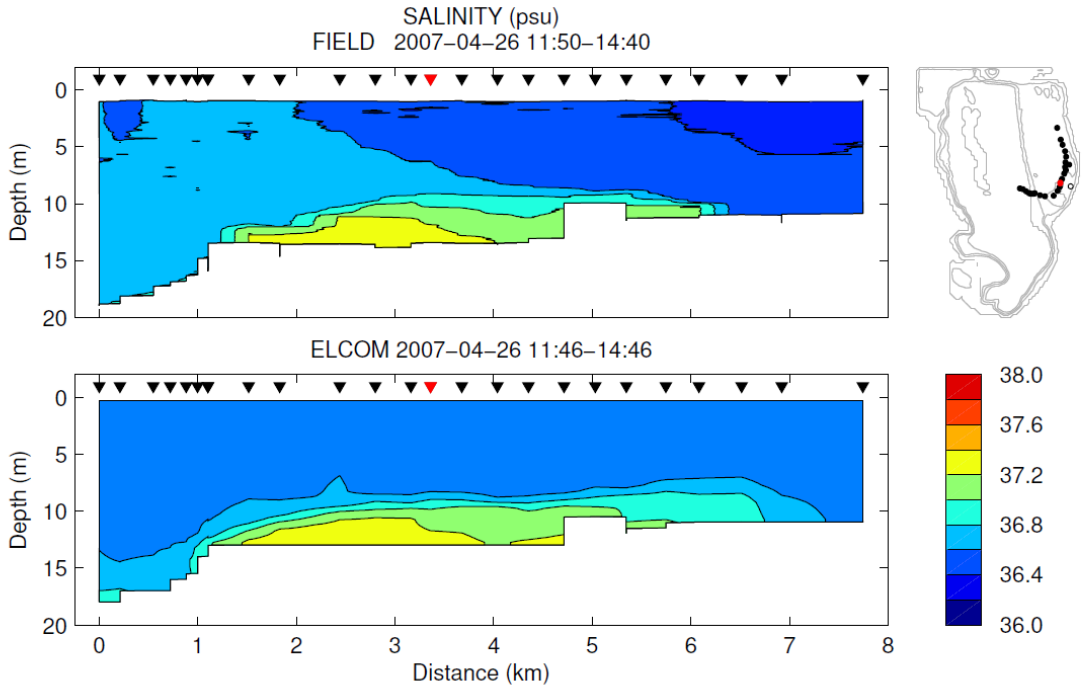

Figure 2-24 Transect of measured (upper panel) and simulated (lower panel) salinity along the main shipping channel and off the shelf during the middle of the day on 26 Apr 2007, 2-5 hours after the dye release (Reproduced from CWR 2007).

Upon further analysis of the data presented in CWR (2007a,b) and additional monitoring undertaken by Water Corporation, CWR (2008) reached the conclusion that between 0.7% and 7% of the brine discharged reaches the deeper basin of Cockburn Sound, with the remainder being either confined to the shallow eastern basin or mixed throughout the water column before exiting Stirling channel. Further, the analysis showed the effluent plume was not detectable between measurements undertaken between 1.0 km and 1.5 km from its entrance into the deep basin of Cockburn Sound, indicating a good degree of mixing as the plume propagated. The analysis further corroborated Water Corporation's (2013) conclusion that depletion of DO in the deep basin of the Sound is triggered by larger scale natural events, and the impacts of the existing plume on DO are minimal.

2.5 Summary

Cockburn Sound provides an ideal location for industrial, social and environmental services (BMT 2017). Due to its protected nature, and despite being subject to the same climate drivers as the more open waters of the Western Australia's coast, Cockburn Sound displays unique hydrodynamic features. These have been described above and are:

(1) Wind driven circulation and mixing resulting from

  (a) land and sea breezes in summer; and

  (b) storms in winter.

(2) Occurrence of density stratification events, including the aspects of its spatial variability, resulting from:

  (a) the evolution of differences of salinity and temperature between the Sound and adjacent waters under the influence of CSWs, notably in the transition from summer to autumn;

  (b) the effects of the Swan-Canning estuaries discharges over the winter period; and

  (c) the evolution of the existing PSDP discharge plume and how it may affect density within the Sound.

(3) The response of DO resulting from the mixing and stratification described above, particularly over the stratified period in the transition between summer and autumn.

These features, acting in isolation or concert, are known to contribute to the development of environmental conditions within the Sound that are conducive to the depletion of aquatic dissolved oxygen at depth. This depletion has been linked with adverse environmental outcomes. The current commission is therefore focussed on developing numerical tools that not only robustly reproduce these features and the associated deleterious dissolved oxygen outcomes, but also permit the investigation of how, or if, these outcomes might be exacerbated by the delivery of a further brine stream to Cockburn Sound.

3 Nearfield model

The present study adopted a proven computational fluid dynamics (CFD) tool for simulating the near-field behaviour of the existing PSDP discharge. This CFD tool was used to obtain realistic plume characteristics under different ambient current conditions and at the nominal discharge flow rate and salinity provided by Water Corporation. The most important output from the CFD model was the dilution map of the plume at different locations near the diffuser (not just on the seabed), which was then subsequently used for integration with the farfield model (see Section 4). These methods, including the integration approach, are consistent with the published methods of Botelho et al. (2012) and Botelho et al. (2016). Details of the CFD model are presented below.

3.1 Model package

OpenFOAM (Open Field Operation and Manipulation) was adopted as the CFD modelling tool for the diffuser assessment performance. OpenFOAM is developed by Open CFD Ltd (based in the UK). Three advantages of using OpenFOAM are:

- Transparency of code. The user is able to interrogate any aspect of the source code to determine exactly which equations are being used;
- Extension of code. The user is able to write tailored conditions, modify equations, and create new solvers for specific problems; and
- Parallel computation. As the software is licensed under a GNU license, a multi-CPU computer cluster may be used to solve large problems without incurring significant license fees. This translates to significant increases in run speeds for complex models.

BMT has been using OpenFOAM for a significant portion of its CFD work for many years. Projects include reaction chemistry in smelting furnaces, coal dust combustion and explosion modelling, Royal Australian Air Force (RAAF) engine test bunker airflow modelling, tidal turbine hydrodynamics, as well as several diffuser outfall models. This method was applied by BMT to the analysis of several diffusers, for both positively and negatively buoyant discharges. For example, CFD simulations were employed for analysis of the proposed BHPB desalination plant diffuser at Point Lowly, South Australia, as part of the Olympic Dam EIS works. As part of those works, this CFD model was compared to experimental results of negatively buoyant plumes and yielded excellent results (BMT WBM 2011).

Of relevance to the current scope, the same CFD methods used in this study were also recently deployed in an analysis of the Sepia Depression ocean outfall. Field measurements of plume dilution at that outfall were made using Rhodamine WT (RWT) and then compared to CFD model predictions. Excellent agreement was found between measurements and numerical predictions, therefore validating the CFD model in a real-world setting (BMT WBM 2015). This, in addition to further RWT validation studies undertaken for legal proceedings around a site on the East coast of Australia (details unable to be disclosed), provides a wealth of evidence that the diffuser simulation methods deployed in the Cockburn Sound modelling study are well tested and robust in their predictive capability.

3.2 CFD model setup

3.2.1 Equations

The equations solved in this application of OpenFOAM were configured for steady-state solutions of the flow resulting from an effluent denser than the ambient that is discharged from the outfall nozzles under a prescribed ambient flow. The equations are listed below, where α is the mixing fraction of effluent of density ρ_1 to background fluid of density ρ_2, ϕ is the mass flux vector, C is the concentration of a tracer released from the outfall, ρ is the mixed fluid density, U is the mean velocity vector, ν_t is the turbulent contribution to kinematic viscosity, h is the water depth and p_d a modified pressure field.

$$\nabla \cdot (\phi\alpha) - \nabla^2 \left[\left(D + \frac{\upsilon_t}{Sc_t}\right)\alpha\right] = 0$$

$$\nabla \cdot (\phi C) - \nabla^2 \left[\left(D + \frac{\upsilon_t}{Sc_t}\right)C\right] = 0$$

$$\rho = \alpha\rho_1(1-\alpha)\rho_2$$

$$\phi = \rho U$$

$$\nabla \cdot (\phi U) - \nabla^2\left(\mu_{eff}U\right) - \nabla U \cdot \nabla\mu_{eff} = -(gh\nabla\rho + p_d)$$

$$p_d = p - \rho g h$$

$$\mu_{eff} = \rho\upsilon_{eff} = \rho(\upsilon + \upsilon_t)$$

The model constants are listed in Table 3-1. C assumes a value of 1 at the diffuser nozzles such that the inverse of C can be used to quantify the effluent dilution. Note that the molecular diffusion constant, D, is very small compared to the turbulence induced mass diffusion $\left({}^{\upsilon_t}/_{Sc_t}\right)$ throughout most the model domain. Also, note that the assumed densities consider the background summer conditions as obtained from density calculations at the intake locations.

Table 3-1 Model constants

Parameter	Description	Value
D	Molecular diffusion constant for heat in water	1.4 x 10^{-9} m^2s^{-1}
Sc_t	Turbulent Schmidt number	0.71
υ	Laminar kinematic viscosity	1.0 x 10^{-6} m^2s^{-1}
g	Acceleration due gravity	-9.81 ms^{-2}
ρ_1	Effluent density	1040.5 kg m^{-3}
ρ_2	Ambient density	1025.0 kg m^{-3}
C	Effluent concentration at the nozzle	1.0

3.2.2 Turbulence model

The turbulent contribution to the viscosity υ_t is calculated by a turbulence model which estimates the energy and length scales of the random fluctuations in the flow field. This variable influences the rate of dispersion/diffusion of the plume, in terms of both momentum and brine concentration. As the Reynolds numbers of the plumes are of the order of 100,000 both k-ε and k-ω SST turbulence models were appropriate choices. The k-ω SST model was selected due to its greater stability and reduced sensitivity to initial conditions. Standard model constants were used.

3.2.3 Domain and mesh

The model domain spanned 300 m (N-S axis) by 460 m (E-W axis) by 10.80 m deep (maximum depth) centred on the diffuser. The sea floor was approximated by constant slopes in the direction of the diffuser, based on the local bathymetry. The depth varied between -10.80 m at the western end of the domain (x = -230 m) to -9.70 m at the east end of the domain (x = 230 m). The depths were similar to those at lowest astronomical tide (LAT).

The volume was meshed with 1 m cubic cells, which were then refined near the diffuser ports to define its geometry (note the manifold is buried under the seabed). This initial discretisation at the diffuser ports enforced limiting cell sizes of 15 mm at the ports (Figure 3-1, Figure 3-2).

Accurately calculating the evolution of the predicted plumes is fundamental to the CFD modelling process. To appropriately resolve plume morphology and mixing, a fine mesh around the boundaries of the plumes, where spatial gradients in velocity, density and concentration are high, was required. However, the use of fine mesh through the entire model domain was not tractable and locating the plume to selectively provide this high resolution for each simulation in advance (where plume position responds to applied boundary conditions) was not possible. As such, an automatic mesh refinement strategy was developed for dynamically enforcing resolution where required within the CFD solutions. Specifically, for each simulation, a first pass solution was computed, then the mesh was automatically refined in the regions where spatial gradients exceeded a pre-defined threshold. This refinement process was repeated until predictions converged. This refining process has been developed at BMT over recent years, and has been applied, for example, to the Olympic Dam EIS diffuser modelling (BMT WBM 2011, Botelho *et al.* 2013) for the Port Pirie Transformation Project diffuser modelling (BMT WBM 2014) and more recently for simulation of the Sepia Depression Ocean Outlet (BMT WBM 2015). The mesh refinement steps for this case are shown in Figure 3-3, whereby the initial mesh begun at 2,671,651 cells and was progressively refined to 6,899,063 cells in 8 steps.

Handling of such large domains were achieved by running the simulations in parallel on dedicated 16 processor computing nodes of one of BMT's high-performance-computing (HPC) facilities.

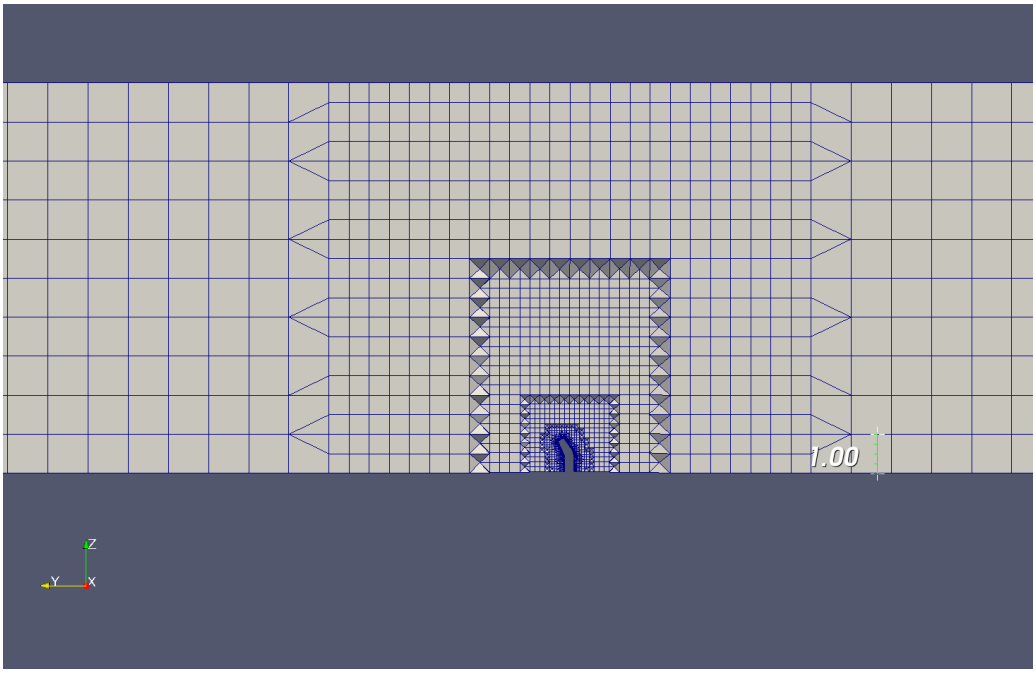

Figure 3-1 Surface mesh showing resolution increase towards the diffuser ports

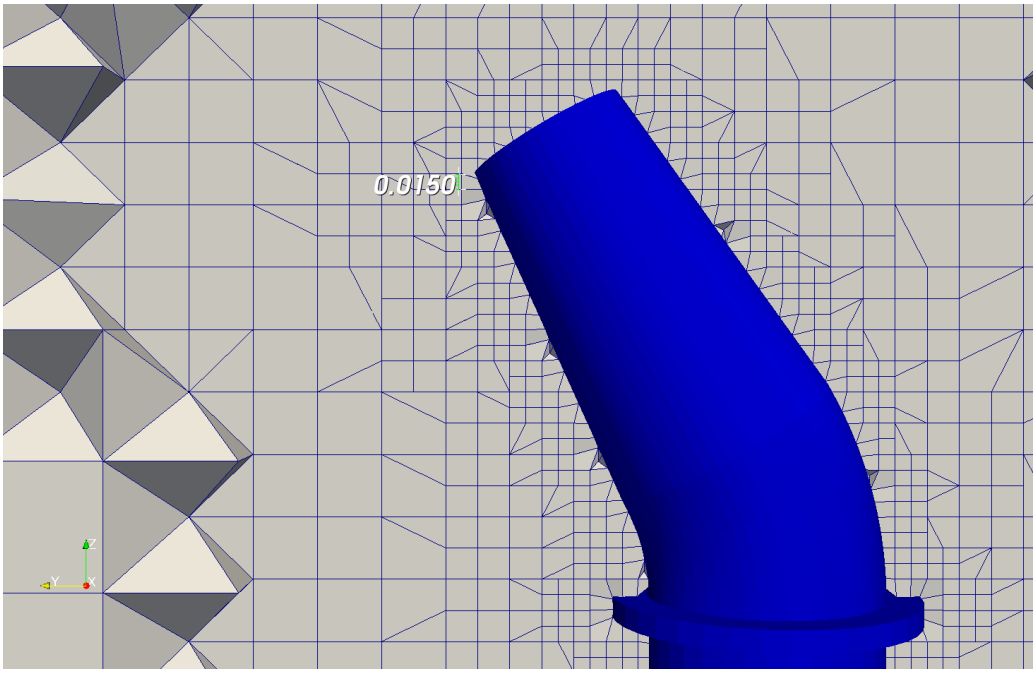

Figure 3-2 Surface mesh at the diffuser ports

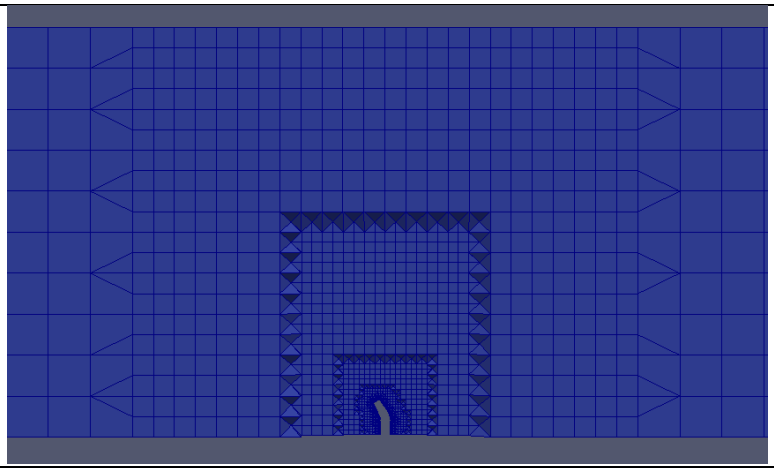

Refinement step 0: 2,671,651 cells

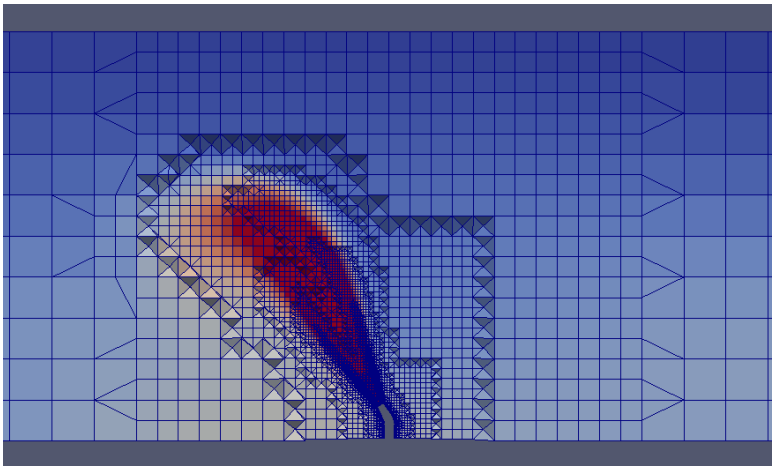

Refinement step 8: 6,899,063 cells

Figure 3-3 Adaptive mesh refinement

3.2.4 Boundary conditions

The bottom surfaces of the model (including diffuser walls and cylindrical surfaces of nozzles) were defined as walls (velocity vector equals 0), against which standard wall functions were used in the turbulence model. The top surface of the model was defined as a 'slip wall', which has no friction but constrains the flow to be parallel to the surface. The remaining field variables were defined as zero-gradient against the top and bottom boundaries. The change in water surface elevation was not accounted for in the CFD model.

The north, east, south and west walls of the domain were specified as inlets and outlets. For each ambient flow case, two of these boundaries were specified as inlets with a fixed velocity vector, and the other two were set to be corresponding outlets with zero- (horizontal) gradient imposed on velocity.

The boundary conditions for α and C were such that they were defined as zero at inflow boundaries, and zero- (horizontal) gradient for the outflow boundaries.

The remaining variables (p_d and turbulence parameters) were defined as zero-gradient.

3.2.4.1 Ambient currents and outfall discharge

The nearfield CFD simulations were designed to cover a wide range of ambient flow conditions and the average diffuser and intake flow rates agreed with Water Corporation. The background ambient currents were specified to cover a range between 0.0 m/s and 0.10 m/s. A total of 9 ambient velocity magnitudes were considered (Table 3-2, four in one shore-parallel direction, four in the other and zero velocity conditions). A single ambient density was considered (Table 3-2).

Table 3-2 Boundary conditions considered in the CFD simulations

Ambient velocity magnitude (m/s)	Discharge flow rate (m^3/s)	Discharge density (kg/m^3)	Ambient density (kg/m^3)
0.00	2.50	1040.5	1025
0.03			
0.05			
0.07			
0.10			

To optimise computational resources, only northeasterly and southwesterly velocities were simulated within the CFD model, noting these as the prevailing preferential longshore flow directions.

Finally, the outflow at each port was assumed to be constant (i.e. it was assumed there was no head loss along the outfall diffuser). The resulting outflows for the individual ports were 62.5 L/s. For each port the outflow was assigned as a velocity vector parallel to the port axis applied to cell faces defining the nozzle exit. The magnitude of the velocity vector was computed by the CFD solver using the specified flow rate and the total projected area of the cell faces. A tracer concentration equal to 1.0 was assigned at each of the diffuser ports.

3.3 Model results

Model results showing the 20:1 iso-surface dilution for all simulated conditions are presented in Figure 3-4 (other iso-dilution surfaces of 10:1, 30:1 40:1 and 50:1 are presented in Appendix A). The iso-surface dilution presentation style was adopted to reveal the shape of the plume in three dimensions. To place these results in some context, a dilution of 20 is the equivalent of a salinity increase of approximately 1.25 for a discharge salinity of 61.4 and ambient salinity of 36.5 (e.g. see Section 2.4).

CFD predictions show that the effluent plume tended to deflect towards the direction of the ambient flow (i.e. towards the northeast or southwest, depending on ambient conditions). At this dilution, the simulated plumes from each port presented little interaction for northwest velocity directions. For south-westerly flows, however, each of the plumes folded onto themselves as a result of the orientation of the ports. This folding resulted in less efficient mixing and a degree of interaction between individual plumes. The lesser degree of mixing for south-westerly flows was manifested by the thicker plumes (i.e. these plumes undergo a slower rate of dilution) in Figure 3-4. These however did not reach as far from the diffuser as the north-easterly velocity cases.

It is also clear from Figure 3-4 that the higher the ambient velocity the more noticeable the deflection (and higher the dilution) of the effluent plume (i.e. the iso-surface became progressively thinner with higher ambient velocities), as expected.

Results of the zero-ambient velocity case were compared against laboratory measurements scaling provided in Roberts and Abessi (2014). This is the most recent publication that specifically addresses the nearfield characteristics of the discharge assuming a multiport linear diffuser, as the one adopted for the PSDP discharge. To BMT's knowledge, no similar relationships have been derived for non-zero ambient currents. A schematic diagram of the nearfield characteristics provided by the Roberts and Abessi (2014) scaling is shown in Figure 3-5.

The different variables given in the diagram were as follows:

- x_i: impact point of the plume
- x_n: length of nearfield
- y_o: port height
- y_t: terminal rise height of the plume
- y_L: thickness at the end of the nearfield (not provided in Roberts and Abessi (2014)
- S_i: dilution at the impact point
- S_n: dilution at the end of the nearfield.

The scaling relationships applicable for the PDSP discharge are as follows.

$$\frac{y_t}{dF} = 1.9\left(\frac{s}{dF}\right)^{1/2}$$

$$\frac{x_i}{dF} = 2.0\left(\frac{s}{dF}\right)^{1/2}$$

$$\frac{x_n}{dF} = 6.0\left(\frac{s}{dF}\right)^{1/2}$$

$$\frac{S_i}{F} = 0.9\left(\frac{s}{dF}\right)$$

$$\frac{S_n}{F} = 1.1\left(\frac{s}{dF}\right)$$

where s is the spacing between the ports, d is the diameter of the points, and F is the port densimetric Froude number, given by:

$$F = \frac{U}{\left(dg\frac{\rho-\rho_o}{\rho_o}\right)^{1/2}}$$

where U is the port exit velocity, g is the acceleration due to gravity, ρ is the brine density, and ρ_o is the ambient density.

Nearfield model

Ambient velocity	North-easterly ambient flow	South-westerly ambient flow
0.00	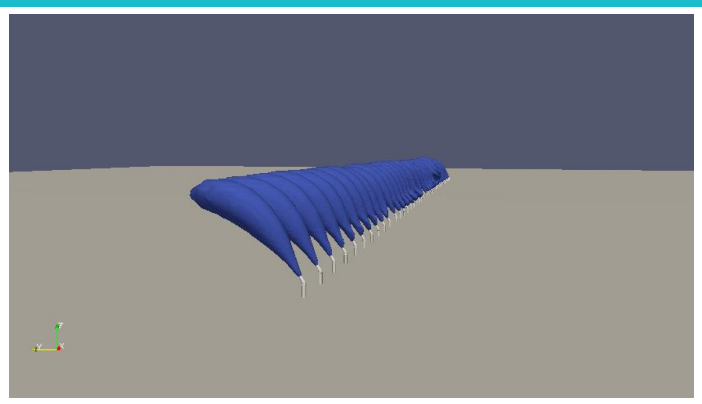	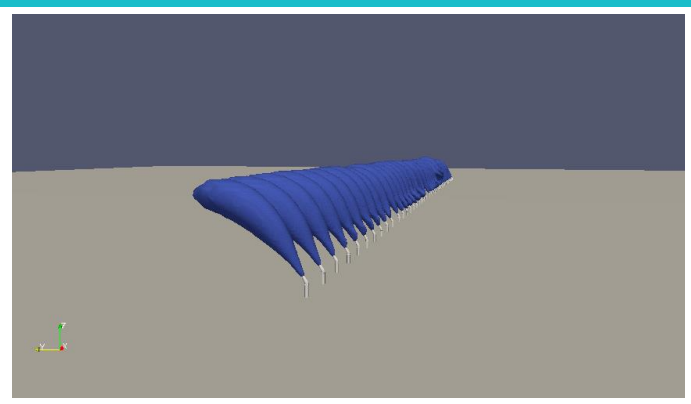
0.03	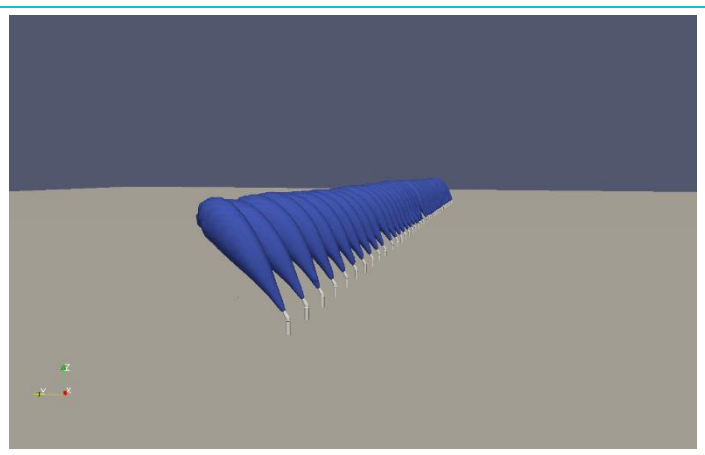	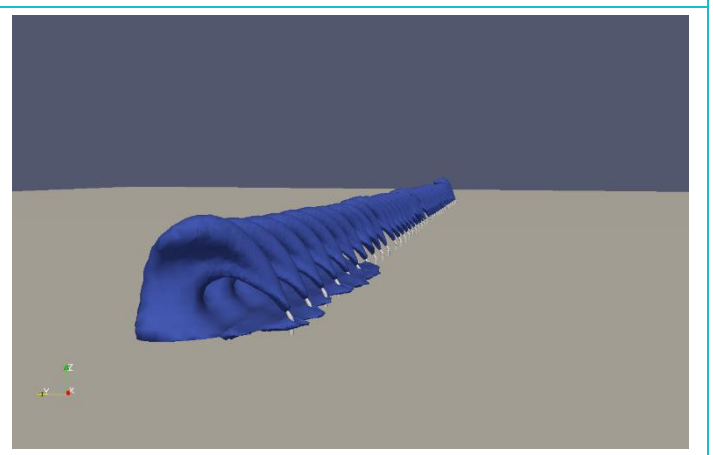
0.05	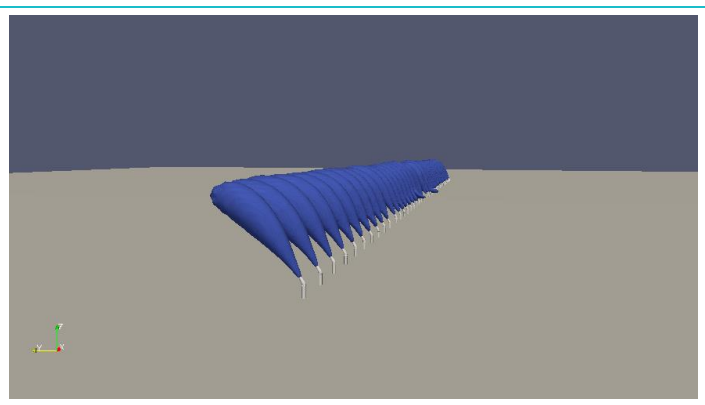	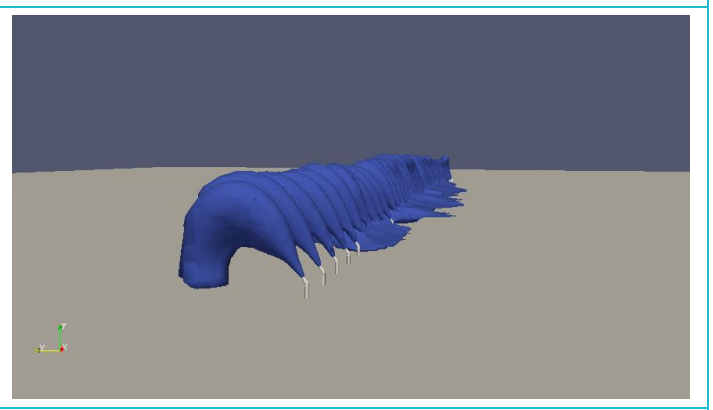
0.07	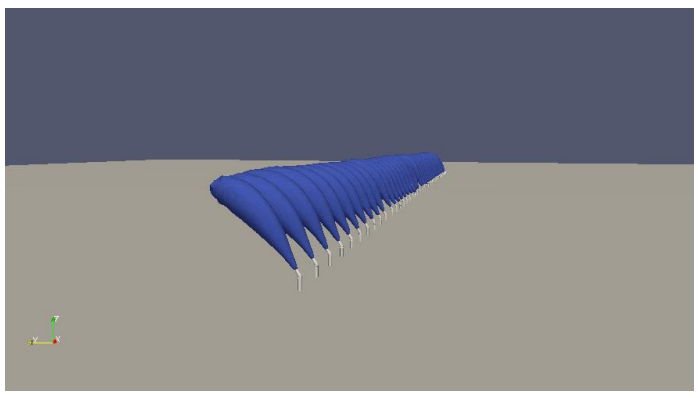	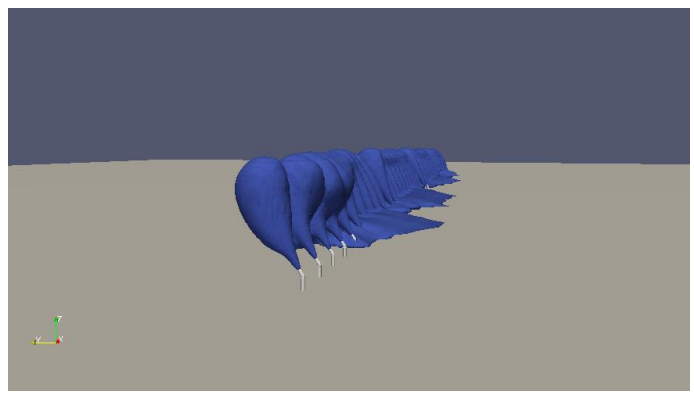
0.10	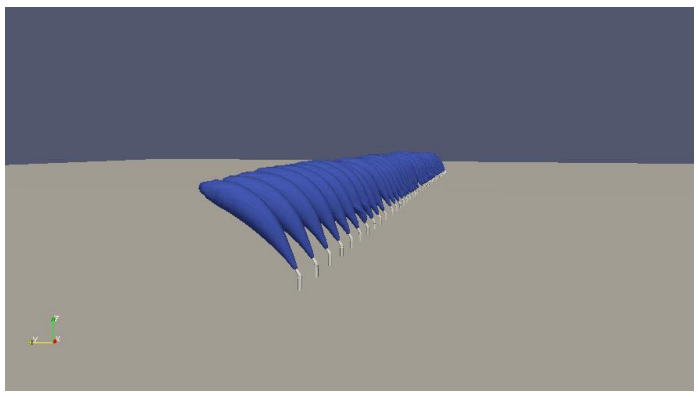	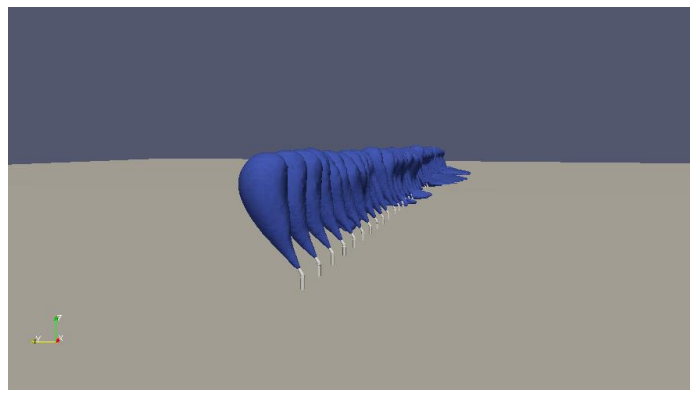

Figure 3-4 Effluent plume resulting from CFD simulations. Results depict the 1:20 iso-surface dilution

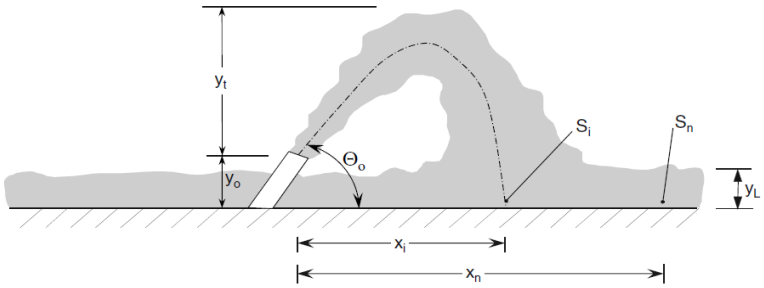

Figure 3-5 Definition diagram for nearfield characteristics (reproduced from Roberts et al. 1997)

A cross-section of the concentration field across port number 25 (i.e. from northwest to southeast) was obtained (Figure 3-6) to extract the values for comparisons with Roberts and Abessi (2014) scaling (Table 3-3). Model results obtained were within the margin of error of the experiments (order of 20%), and generally slightly more conservative in terms of dilutions (i.e. the model predicted marginally lower dilutions at comparable distances from the diffuser.

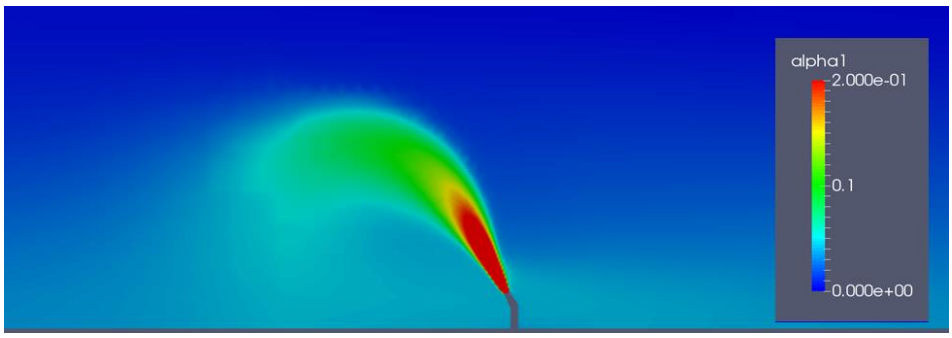

Figure 3-6 Cross-section illustrating brine concentration field for comparisons with Roberts and Abessi (2014) scaling

Table 3-3 Comparison of model results with Roberts and Abessi (2014) scaling

Variable	Model results	Roberts and Abessi (2014) scaling
s	4.0 m	4.0 m
d	0.13 m	0.13 m
F	34.5	34.5
s/dF	0.89	0.89
x_i	6.5 m	8.5 m
x_n	(see note 1)	25.4 m
y_t	7.6 m	8.0 m
S_i	25.2	27.7
S_n	33.6 (see note 2)	33.8
Note 1: x_n was not given as based on velocity fluctuations not provided by the model Note 2: S_n in the model provided at 25.4 m from the port.		

3.3.1 Dilutions in the nearfield

Of relevance to the assessment presented in this study, are the dilutions (and hence salinities) in the intermediate field. In this case, minimum dilutions were extracted at the end of the nearfield (Table 3-4) to show the degree of mixing achieved in the nearfield. In this case, the end of the nearfield (x_n) was assumed to be the same as the case of zero ambient velocity as provided by the Roberts and Abessi (2014) scaling. This distance was assumed to be in the direction of the ambient flow and the dilution values were the lowest in the water column at x_n.

Table 3-4 shows that for north-easterly directions, lower ambient currents delivered lower dilutions. For south-westerly currents, the shape and trajectory of the effluent plume influenced mixing of the plume considerably. For these currents, dilutions reduced between 0.03 m/s and 0.05 m/s, and increased again for higher ambient velocities. Dilutions were higher than 25 for all ambient currents.

Table 3-4 Minimum dilutions at the end of nearfield (25.4 m from the diffuser) obtained from CFD simulations

Current speed (m/s)	Minimum dilution (-)
0.00	33.6
0.03 (NE)	29.6
0.05 (NE)	30.0
0.07 (NE)	31.7
0.10 (NE)	35.3
0.03 (SW)	34.0
0.05 (SW)	28.5
0.07 (SW)	35.3
0.10 (SW)	41.4

The dilutions in Table 3-4 can also be contrasted to the nearfield measurements shown in CWR (2007a) presented in Figure 2-22, which shows an average dilution at 25 m from the diffuser equals approximately 50. For the conditions on the day, CWR (2007a) indicates the local currents were 0.06 m/s towards the north. The dilution equal to approximately 30 indicated the CFD model underpredicted dilutions. However, the difference between dilution estimates can be expected noting CWR (2007a) values were averaged between all measured profiles, discharge flow rates on the measurement day were different to those modelled in this study, and the reported CFD results were the minimum dilutions. CFD results can be considered conservative compared to the field measurements (i.e. provide a lower dilution).

4 Farfield model

A coupled hydrodynamic and water quality model was constructed to simulate dispersion of both the existing and proposed future return waters, once they are under conditions that are no longer influenced by the initial momentum and buoyancy of the discharge plumes. These conditions are known as farfield and are generally simulated with relatively large-scale hydrodynamic models (e.g. the model domain is more than ten thousand times larger than the diffuser length, e.g. Botelho et al. 2016).

This section presents the coupled hydrodynamic and water model of Cockburn Sound to be used for assessment of future discharge scenarios. Scenario assessments are not part of the scope of works covered by this report.

4.1 Water quality model (AED2)

The Aquatic Ecosystem Model version 2 (AED2, Hipsey et al., 2013) was coupled to TUFLOW FV to simulate dissolved oxygen in Cockburn Sound. AED2 is developed by A/Professor Matthew Hipsey at the University of Western Australia. Coupled TUFLOW FV and AED2 models have been adopted for a number of coastal and estuarine studies, including:

- Abrolhos Islands for Mid West Aquaculture Zone (2014-2015)
- Simulation of the fate and transport of bacteria within effluent discharged at Sepia (2015-2017)
- The Hawkesbury-Nepean River (2011-14)
- The Yarra River (2012- ongoing)
- Lake Samsonvale, Queensland
- Three-dimensional modelling of Moreton Bay and every major estuary (a total of 17 estuaries) in Southeast Queensland from Currumbin Creek in the south to the Noosa River in the north (2014 -ongoing).

In AED2, dissolved oxygen dynamics account for atmospheric exchange, sediment oxygen demand, microbial consumption during organic matter mineralisation and nitrification, photosynthetic oxygen production and respiratory oxygen consumption, and respiration by other optional biotic components (Figure 4-1, adapted from Hipsey et al. 2013).

Whilst TUFLOW FV was used to calculate water levels and both advection and diffusion of scalars (temperature, salinity and DO), AED2 was applied to calculate source and sink terms specific to the DO dynamics. A simplified AED2 configuration was adopted in which only atmospheric exchange and SOD were modelled (first two terms in the right-hand side of the main equation in Figure 4-1. This simplification was justified based on previous modelling undertaken in Cockburn Sound, which indicated these were the dominant DO sources and sinks (CWR 2006). Atmospheric exchange was based on the model of Wanninkhof (1992) and the flux equation of Riley and Skirrow (1974). A simple SOD flux that varied as a function of the overlying water temperature and limited by dissolved oxygen concentration in the bottom water was adopted.

State variable mass balance equation:

$$\frac{dO_2}{dt} = \pm f_{atm}^{O_2} - f_{sed}^{O_2} - \frac{f_{miner}^{DOC}}{\chi_{C:O_2}^{miner}} - \frac{f_{nitrif}}{\chi_{N:O_2}^{nitrif}} + \sum_{a}^{N_{PHY}} \left(\frac{f_{uptake}^{PHY\_C_a}}{\chi_{C:O_2}^{PHY}} \right) - \sum_{a}^{N_{PHY}} \left(\frac{f_{resp}^{PHY\_C_a}}{\chi_{C:O_2}^{PHY}} \right) - \sum_{z}^{N_{ZOO}} \left(\frac{f_{resp}^{ZOO_z}}{\chi_{C:O_2}^{ZOO}} \right)$$

= ± atmospheric O_2 exchange
± sediment O_2 demand
– O_2 consumption by mineralisation of DOC (bacterial respiration)
– O_2 consumption by nitrification
+ O_2 production by photosynthesis
– O_2 consumption by phytoplankton respiration
– O_2 consumption by zooplankton respiration

Process parameterisations:

$$f_{atm}^{O_2} = \begin{cases} \frac{c_{atm}^{O_2}([O_2]_{atm} - [O_2]_z)}{dz_s} & if\ z = z_s \\ 0 & if\ z \neq z_s \end{cases}$$ atmospheric oxygen exchange

$$f_{sed}^{O_2} = F_{max}^{O_2} \frac{O_2}{K_{sed}^{O_2} + O_2} \left(\theta_{sed}^{O_2}\right)^{T-20} \left(\frac{\widehat{A_z}}{dz_z}\right)$$ sediment oxygen demand (SOD)

where $\widehat{A_z} = A_z^{ben}/A_z$ and dz_z is the thickness of the z^{th} layer/cell.

Figure 4-1 AED2 dissolved oxygen governing equations

4.2 Hydrodynamic model (TUFLOW FV)

The hydrodynamic modelling component of these assessments was undertaken using the TUFLOW FV software, which is developed and distributed by BMT. TUFLOW FV is a numerical hydrodynamic model for the two-dimensional (2D) and three-dimensional (3D) Non-Linear Shallow Water Equations (NLSWE). The model is suitable for simulating a wide range of hydrodynamic systems ranging in scale from open channels and floodplains, through estuaries to coasts and oceans. The three-dimensional model was deployed in this study.

The Finite-Volume (FV) numerical scheme employed by TUFLOW FV solves the NLSWE on both structured rectilinear grids and unstructured meshes comprised of triangular and quadrilateral elements. The flexible mesh allows for seamless boundary fitting along complex coastlines or channels as well as accurately and efficiently representing complex bathymetries with a minimum number of computational elements. The flexible mesh capability is particularly efficient at resolving a range of scales in a single model without requiring multiple domain nesting, such as the case with the PSDP discharge modelling.

4.3 Model domain, mesh and bathymetry

The hydrodynamic model domain is shown in Figure 4-1 and extends from Cape Naturaliste in the south to Cervantes in the north, covering approximately 400 km of coastline. Offshore the model extends approximately 140 km into the Indian Ocean to depths greater than 4,000 m.

The model consists of 16,014 horizontal mesh cells with characteristic dimensions varying from approximately 9.0 km at the offshore boundary, and decreasing to 50 m in the vicinity of the PSDP (and proposed future) outfall diffuser. Figure 4-2 shows a detail of the model mesh in the study area.

A 10 m digital elevation model (DEM) was generated for the study area from a range of data sources (Table 4-1). In particular, the DEM was supplemented with finer resolution multibeam data over the Australian Marine Complex (AMC), Exit, Parmelia, Success, Calista and Stirling channels provided

by Fremantle Ports Authority (FPA). Data from Geosciences Australia and General Bathymetric Chart of the Oceans (GEBCO) were used to complement the bathymetric information for production of the DEM. Figure 4-2. The final step in the preparation of the model bathymetry consisted of calculating the average value of all DEM points within each cell of the domain and assigning this average as the representative elevation of the seabed at that particular location. Figure 4-3 show the DEM used to represent the model bathymetry.

Table 4-1 Available bathymetric data

Custodian	Date	Description	Vertical datum
DoT	2009	5m LiDAR collected by DoT over the metropolitan region.	AHD
FPA	2003	Multibeam over AMC and exit channels.	LWMF
FPA	2006	Multibeam over Calista and Stirling channels.	LWMF
DoT	2009	Extends the 2009 LiDAR coverage to the north.	AHD
FPA	December 2011	Bathymetry for Deep Water Channel Fremantle.	LWMF
FPA	November 2006	XYZ Sounding Data for FPA's Deep Water Channel North Part.	LWMF
FPA	November 2006	XYZ Sounding Data for FPA's Deep Water Channel South Part.	LWMF
FPA	November 2009	Bathymetry Point dataset around spoil ground area, Gage Road.	LWMF
FPA	March 2010	Bathymetry Point dataset around spoil ground area, Gage Road.	LWMF
FPA	December 2010	Bathymetry Point dataset around spoil ground area, Gage Road.	LWMF
FPA	December 2012	Bathymetry Point dataset around spoil ground area, Gage Road.	LWMF
FPA	November 1991	Parmelia and Success channels surveys.	LWMF
FPA	October 2000	Parmelia and Success channels surveys.	LWMF
FPA	June 2002	Parmelia and Success channels surveys.	LWMF
FPA	March 2003	Parmelia and Success channels surveys.	LWMF
FPA	March 2007	Parmelia and Success channels surveys.	LWMF
FPA	February 2009	Parmelia and Success channels surveys.	LWMF
FPA	February 2012	Parmelia and Success channels multibeam survey.	LWMF
FPA	April 2013	Parmelia and Success channels multibeam survey.	LWMF
FPA	October 2013	Parmelia and Success channels multibeam survey.	LWMF
FPA	March 2015	Parmelia and Success channels multibeam survey.	LWMF
GEBCO	2014	Bathymetric Gridded Surface, 30 second of arc.	MSL
DoT	1994	Bathymetric Gridded Surface 100 m cells, Perth Coastal Waters.	LWMF
DoT	2001	Bathymetric Isobaths Broadscale, WA (polylines).	CD
GA	2005	Bathymetric Isobaths from 250 m grid, Australia.	mAHD
FPA	December 2012	Multibeam Survey IH Disposal Area.	LWMF
LWMF – Low Water Mark at Fremantle and 0.756 m below mAHD			

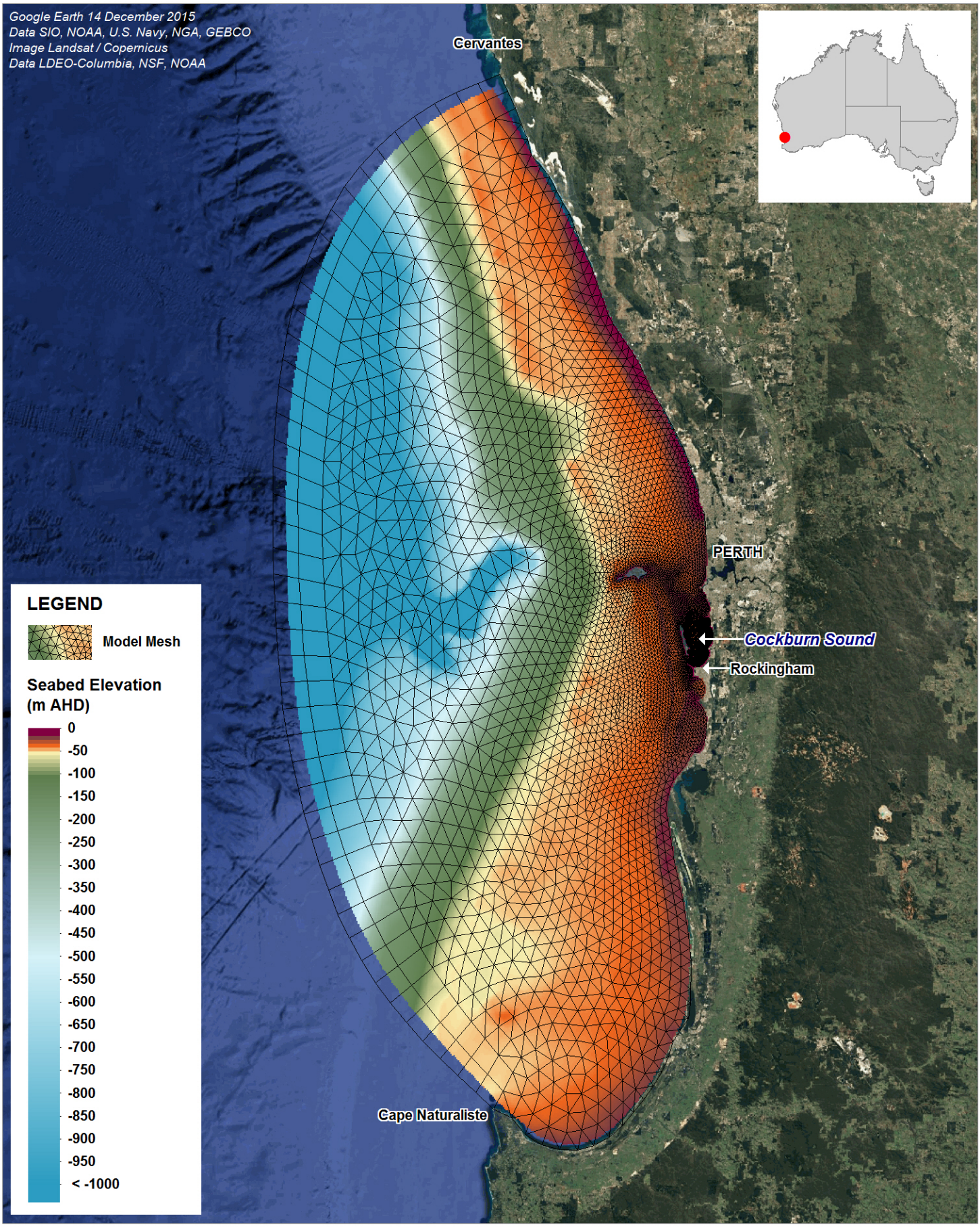

Title:

Hydrodynamic Model Extent and Bathymetry

Figure: **4-2**

Rev: **A**

BMT WBM endeavours to ensure that the information provided in this map is correct at the time of publication. BMT WBM does not warrant, guarantee or make representations regarding the currency and accuracy of information contained in this map.

N

0 40 80km

Approx. Scale

BMT

www.bmt.org

Filepath: I:\B22253.I.meb.CockburnSound\DRG\CAR_004_170927_Hydrodynamic Model Extent and Bathymetry.wor

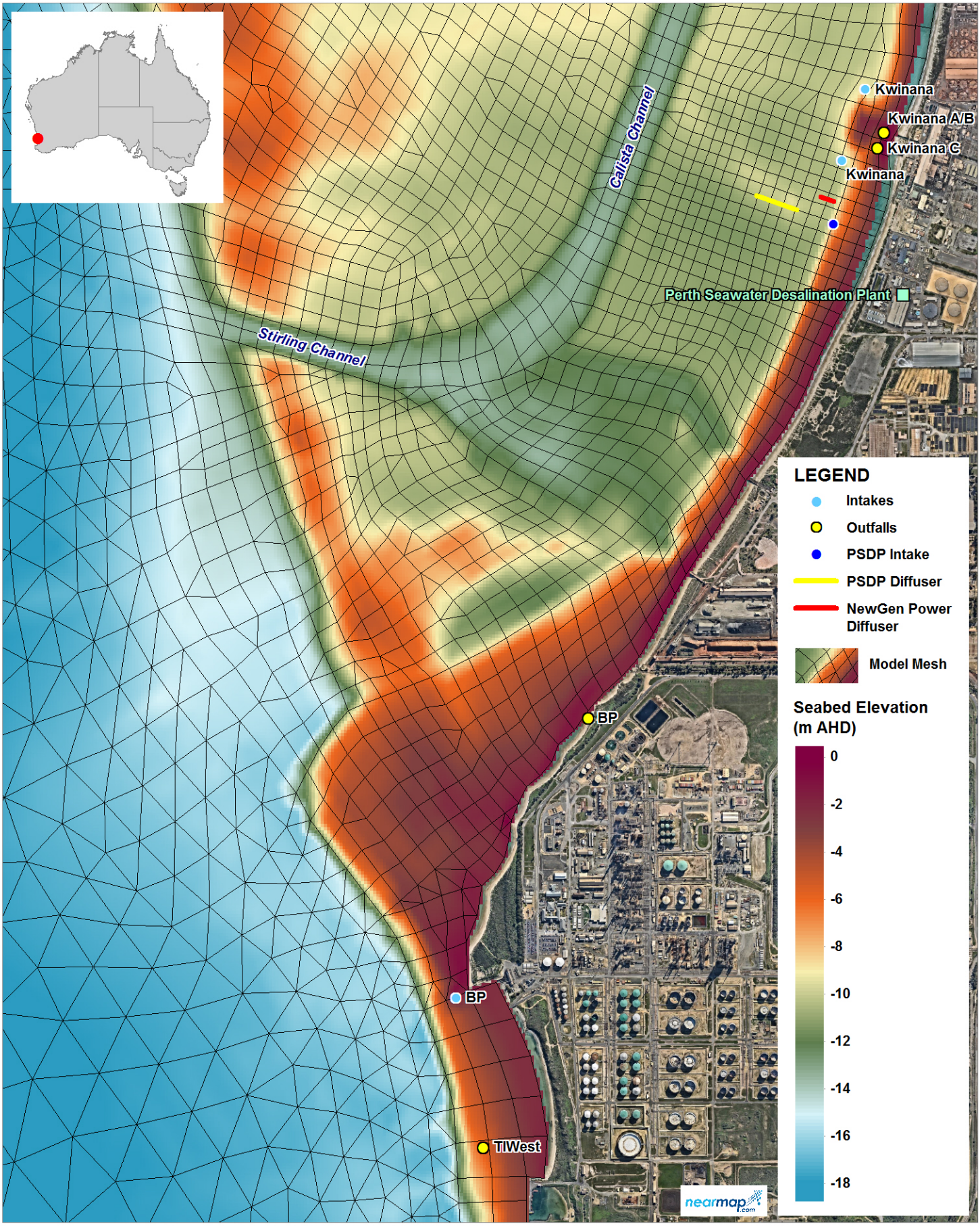

Title:

Hydrodynamic Model Mesh Detail

Figure: **4-3**

Rev: **A**

BMT WBM endeavours to ensure that the information provided in this map is correct at the time of publication. BMT WBM does not warrant, guarantee or make representations regarding the currency and accuracy of information contained in this map.

N

0 400 800m

Approx. Scale

BMT

www.bmt.org

Filepath: I:\B22253.I.meb.CockburnSound\DRG\CAR_005_170928_Hydrodynamic Model Mesh Detail.wor

4.4 Boundary conditions

Details of the specific information sources used to the develop boundary conditions applied to the hydrodynamic model are proved below.

4.4.1 Wind

The extents of the model domain requires specification of a wind field that is representative of both the local area of interest (i.e. Cockburn Sound) and the regions further afield. Previous modelling successfully adopted the local BoM measurements at Garden Island as the wind forcing (CWR 2009). For the areas further afield, particularly offshore, field measurements are not available. However, data from global data assimilation models are readily available and routinely adopted for coastal and oceanic modelling.

In the present study, a combination between the local BoM wind data at Garden Island and data from the global data-assimilation model NCEP Climate Forecast System Version 2 (CFSv2) was adopted. CFSv2 wind data at the grid location nearest to the Garden Island station was shown to correlate reasonably well with BoM data at Garden Island (Figure 4-4). Therefore, and also noting the CFSv2 is product from data-assimilation, use of CFSv2 was deemed suitable for representation of the winds further afield in this study.

Both CFSv2 and BoM data at Garden Island were provided at hourly time intervals. CFSv2 is spatially variable on a 0.205º resolution grid (Figure 4-5). For the combination of the data sets, the CFSv2 wind data at the four grid locations surrounding Cockburn Sound were replaced with the BoM measured data at Garden Island. This ensured that TUFLOW FV was not interpolating CFSv2 wind data from overland locations for subsequent application to Cockburn Sound. Note that the BoM wind direction data shown in May 2006 was compromised (Figure 4-4), as such wind direction data from CFSv2 at nearest location to the BoM station was used to complement the BoM wind direction data.

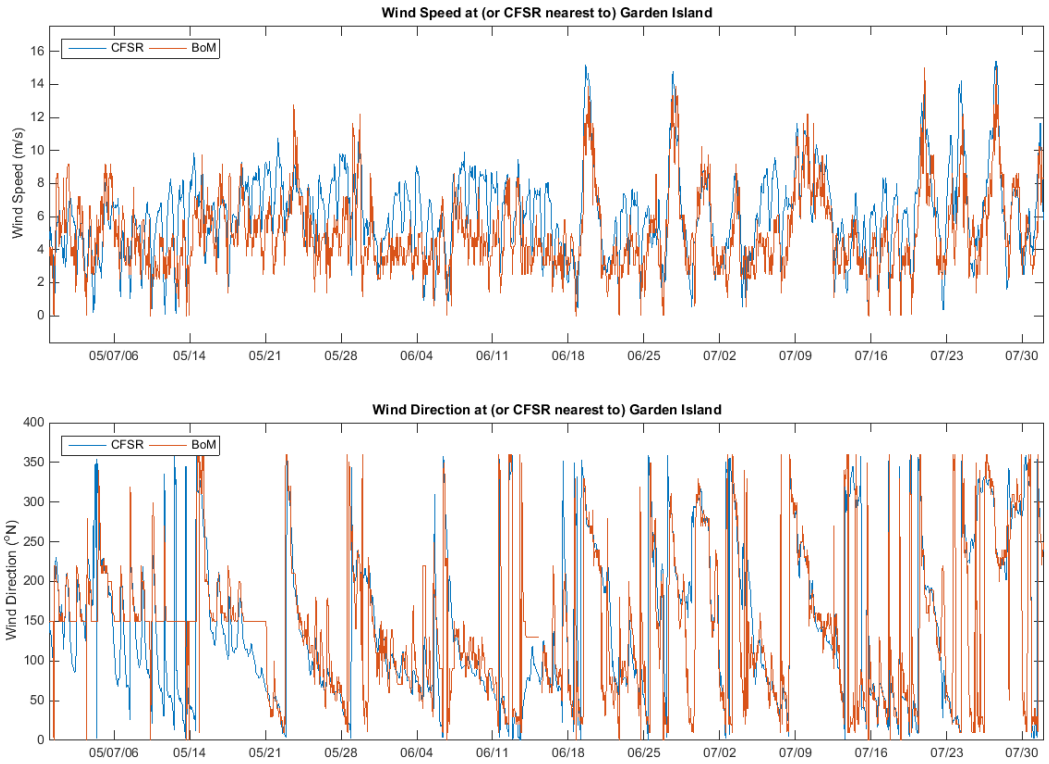

Figure 4-4 Comparison between Garden Island and CFSv2 wind data at nearest grid location

4.4.2 Tides

Due to the large extent of the model domain, tidal elevations varied spatially and temporally along the length of the offshore boundary. Tidal data were sourced from the global tidal model TOPEX (TPX08-atlas, Egbert and Erofeeva, 2002). The TOPEX data are available globally in a 1/30° resolution. The locations at which TOPEX data were sourced are respectively shown in Figure 4-6. Note, however, that only the data around the model open boundary were relevant for the simulations required of this study.

4.4.3 Regional currents, salinity, temperature, and DO

The model was provided with regional current forcing (residual water level, current magnitude and direction), temperature and salinity profiles at the open boundary. These data were sourced from the HYCOM + NCODA Global 1/12° Analysis data assimilation system (Cummings and Smedstad, 2013). HYCOM is an abbreviation for HYbrid Coordinate Ocean Model and NCODA is an abbreviation for Navy Coupled Ocean Data Assimilation. The HYCOM + NCODA data are available globally in a 1/12° resolution. The locations at which HYCOM + NCODA data were sourced are respectively shown in Figure 4-7. The residual water level from HYCOM + NCODA was added to the astronomical tide data from TOPEX (see Section 4.4.2) to form the final specification of water levels at the open boundary conditions.

The DO boundary condition across the water column was assumed to be at 100% saturation based on the temperature and salinity data using the formulas given in Riley and Skirrow (1974).

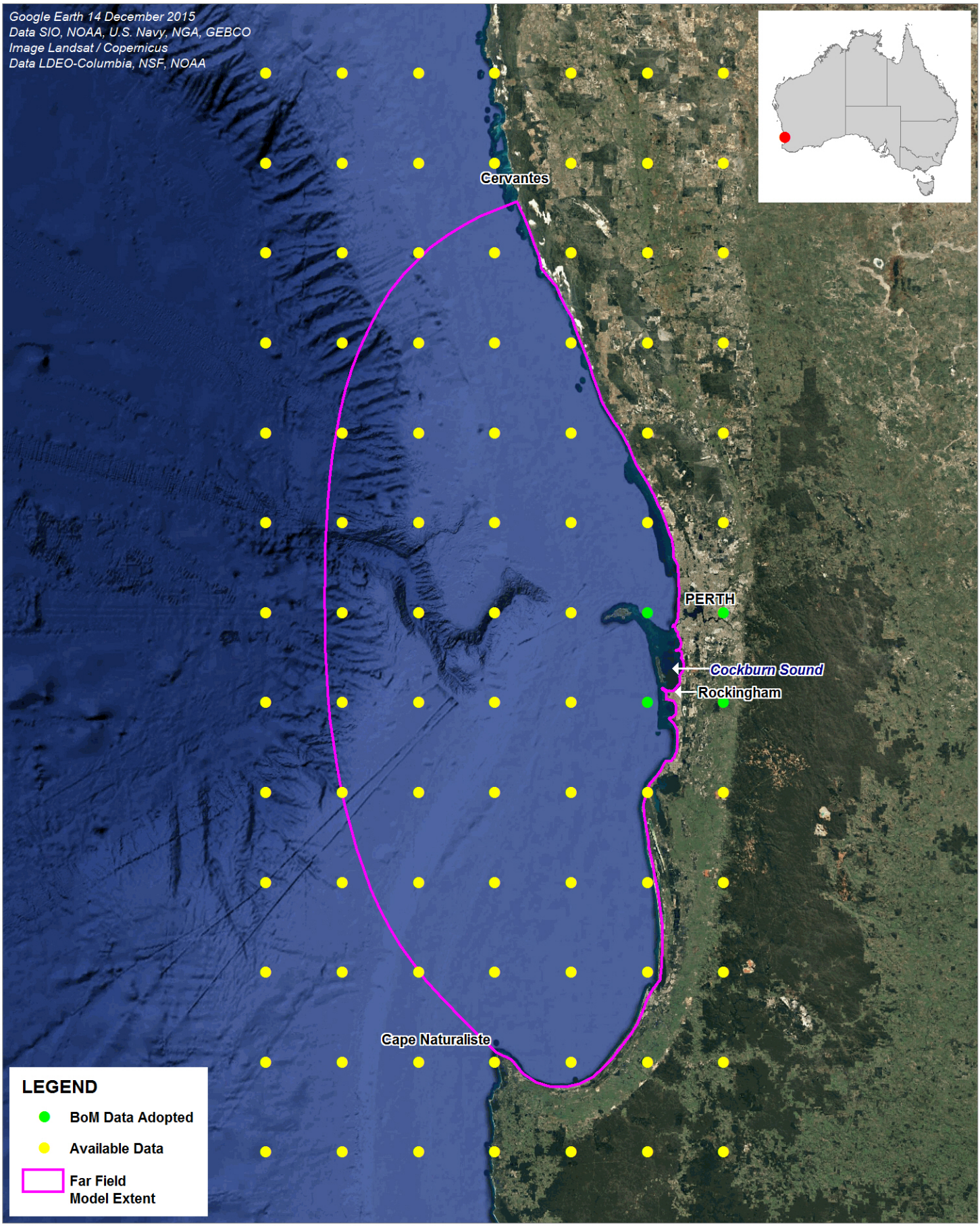

Title:

Locations where CFSv2 Data were Available

Figure: **4-5**

Rev: **A**

BMT WBM endeavours to ensure that the information provided in this map is correct at the time of publication. BMT WBM does not warrant, guarantee or make representations regarding the currency and accuracy of information contained in this map.

N

0 50 100km

Approx. Scale

BMT

www.bmt.org

Filepath: I:\B22253.I.meb.CockburnSound\DRG\CAR_008_170929_Locations where CFSv2 Data Were Available.wor

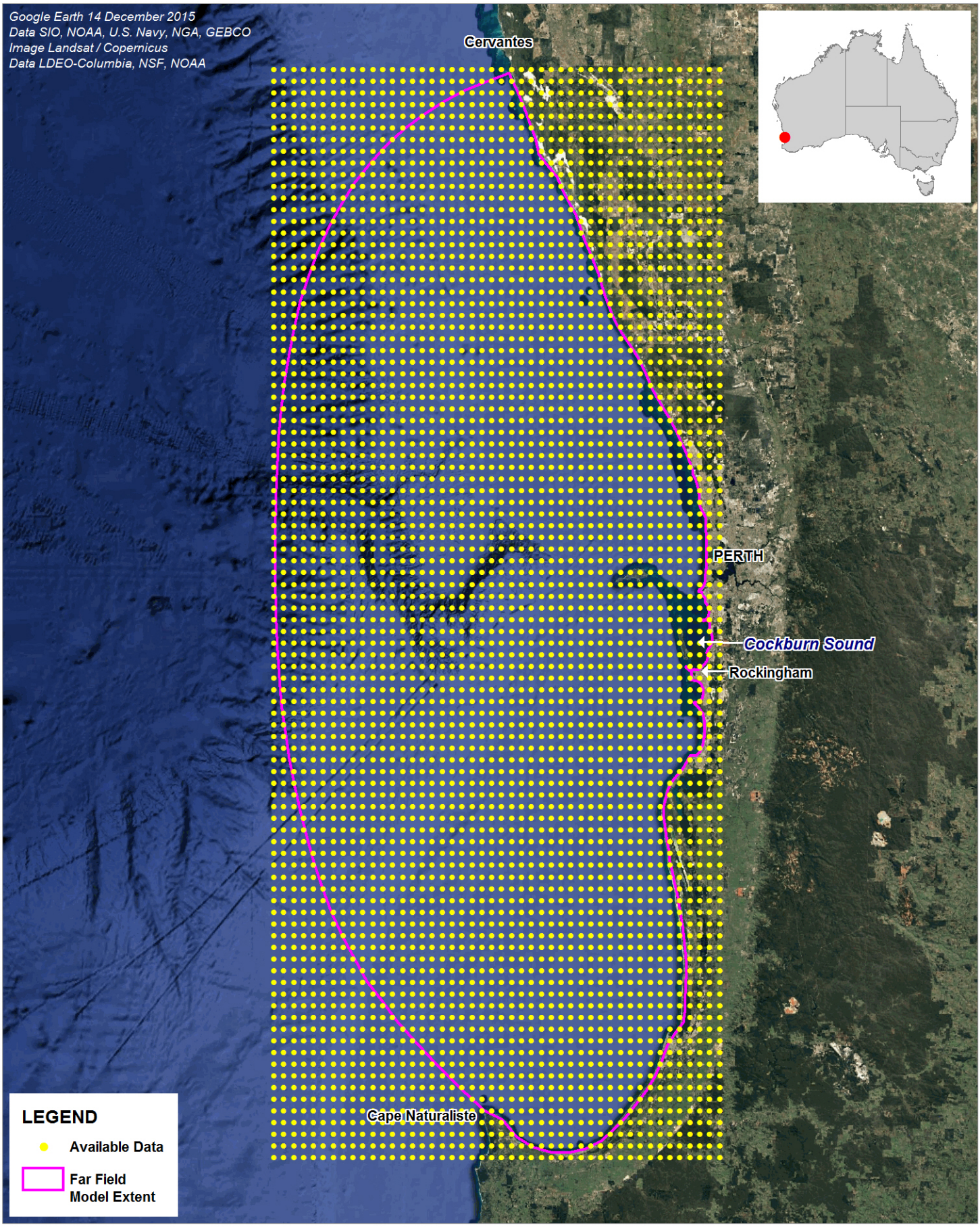

Title:

Locations where TOPEX Data were Available

Figure: 4-6

Rev: A

BMT WBM endeavours to ensure that the information provided in this map is correct at the time of publication. BMT WBM does not warrant, guarantee or make representations regarding the currency and accuracy of information contained in this map.

N

0 40 80km

Approx. Scale

BMT

www.bmt.org

Filepath: I:\B22253.I.meb.CockburnSound\DRG\CAR_009_170929_Locations where TOPEX Data Were Available.WOR

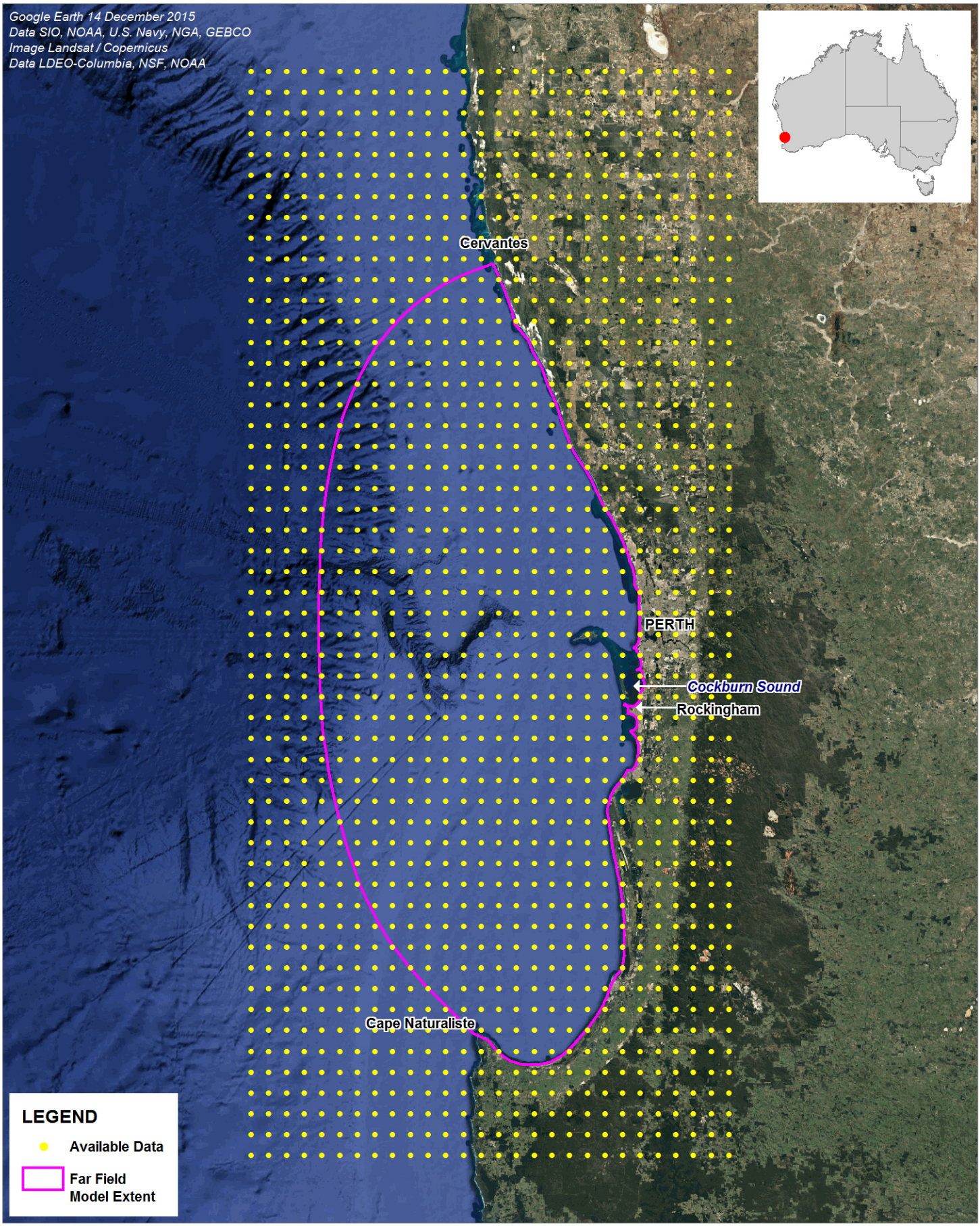

Title:

Locations where HYCOM + NCODA Data were Available

Figure: 4-7

Rev: A

BMT WBM endeavours to ensure that the information provided in this map is correct at the time of publication. BMT WBM does not warrant, guarantee or make representations regarding the currency and accuracy of information contained in this map.

N

0 50 100km

Approx. Scale

BMT

www.bmt.org

Filepath: I:\B22253.I.meb.CockburnSound\DRG\CAR_010_170929_Locations Where HYCOM + NCODA Data Were Available.WOR

4.4.4 Radiation, precipitation and humidity

Water column heat dynamics were simulated directly within TUFLOW FV. Long and short wave radiation, precipitation and relative humidity forcing data were derived from global NCEP model reanalyses and applied to TUFLOW FV to support its simulation of water column heat dynamics. These model input fields were spatially uniform (i.e. gridded) but varied in time in order to represent both seasonal and higher-frequency variations (e.g. diurnal, weekly, etc.). The locations at which these data were sourced and applied are shown in Figure 4-5.

4.4.5 Air temperature

Air temperature was not sourced from NCEP reanalysis data, as this was shown to be of poor quality when compared to local data (BMT WBM 2017a). Air temperature from the BoM station at Garden Island was therefore adopted in the model.

4.4.6 Swan River flows

Winter simulations (Section 5.3) included freshwater flows draining to the Swan-Canning River catchment. At other times, Swan River discharges were generally below 5 m^3/s and therefore deemed negligible for the purposes of this modelling study. The boundary condition for the Swan River flows was located at the cell adjacent to the estuary mouth in Fremantle.

Flow, temperature and salinity data are not available at the Swan River mouth for specification of the boundary conditions. To overcome this limitation, and account for the effects of the tidal elevations, flow data was generated from a separate, calibrated, hydraulic model. This model considered the effects of tides as well as catchment flows and direct surface run-off from local catchments into the Swan River. This hydraulic model has recently been used to execute the Swan flood study (undertaken by BMT) and its details are provided Appendix B.

Figure 4-8 shows the recorded Swan River flow rate at Walyunga (converted from site rating curve), and the modelled discharge at the Swan River mouth at Fremantle as applied as the boundary to the TUFLOW FV model.

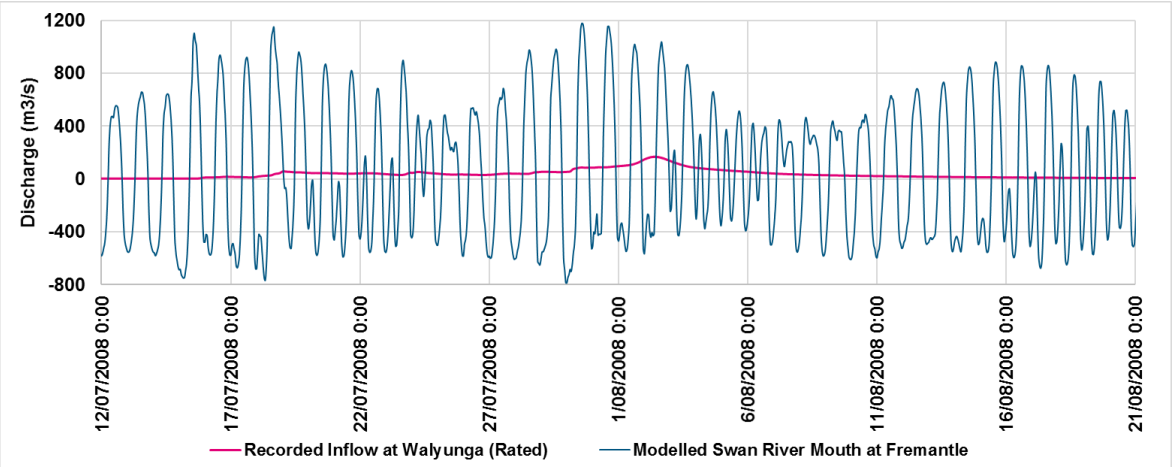

Figure 4-8 Swan River Flows

The Cockburn Sound model was found to be sensitive to the temperature and salinity specification adopted at the Swan River inflow boundary. Field data in the Sound was used to guide the specifications of these boundary conditions in the model. A time series of the adopted temperature and salinity applied at the Swan River mouth is shown in Figure 4-9. A DO saturation of 100% based on temperature and salinity (Riley and Skirrow 1974) at the location obtained from a simulation without the Swan inflow were assumed for the boundary conditions.

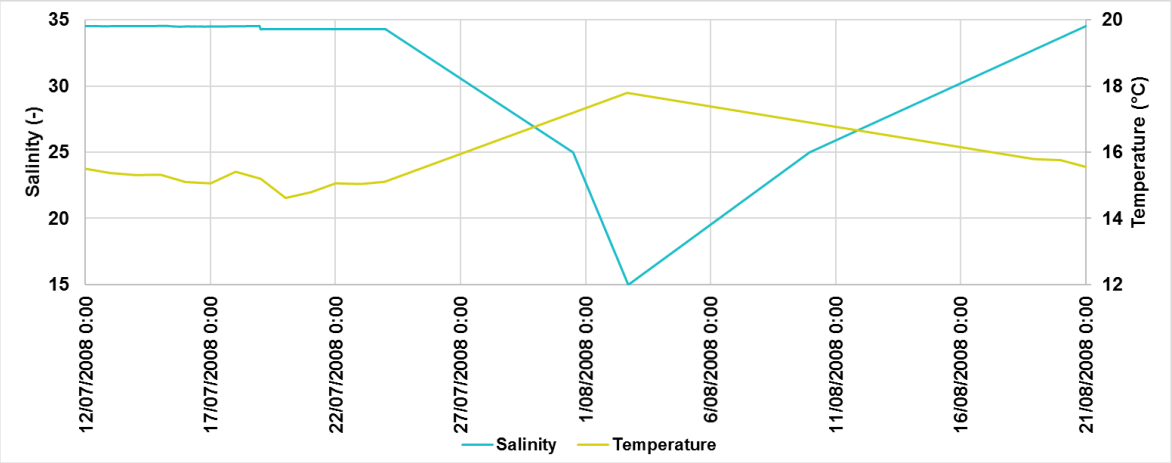

Figure 4-9 Temperature and Salinity Specification at Swan River Mouth

4.4.7 PSDP discharge

4.4.7.1 Modelling approach

Brine mixing near an outfall is dominated by diffuser-induced vertical momentum and buoyancy. In this region, flow generally undergoes considerable vertical accelerations associated with both the initial discharge momentum through a relatively narrow nozzle and the buoyancy effects associated with the density difference between brine and the ambient water. These strong vertical accelerations induce fine-scale turbulence through shearing and are responsible for the enhanced mixing generated by the diffuser. Importantly, the hydrodynamics associated with this shearing motion occur at relatively small spatial scales (0.001 to 10 metres) when compared to the scales of the ambient farfield motion (100 to 1000s metres) and are inherently non-hydrostatic. Therefore, both the need to resolve small scale process and include non-hydrostatic simulation in traditional farfield models makes simulation of diffusers with these tools problematic. This is one reason CFD modelling of these dynamics was undertaken in this study (see Section 3).

Given that it is impractical to simulate the entire farfield domain using CFD, and that farfield models cannot properly resolve detailed mixing processes around diffusers, separate models must be selected for each, and then linked. This approach has been taken in this study. Specifically, the nearfield model presented in Section 3 was linked to TUFLOW FV for the subsequent simulation of brine dispersion from the PSDP outfall. The methods used to do so in this study are described below and further details are provided in Appendix I.

4.4.7.2 Linkage technique

Different linkage techniques between near and farfield have been adopted for assessments of the effluent discharge dispersion from outfalls (e.g. Marti *et al*. 2011, Botelho *et al.* 2013, BMT WBM 2014, Botelho *et al.* 2016). Botelho *et al.* (2013) defined a series of characteristics required for the linkage between the models, including:

- Effluent mass conservation – This is required to ensure the mass of effluent discharged by the outfall is conserved.
- Controllable linkage with nearfield predictions - It is necessary to ensure that the boundary condition flows (and hence dilutions and effluent concentrations) at the site of the diffuser are not artificially determined by the cell sizes and time steps of the hydrodynamic (farfield) model for subsequent advection and dispersion through its domain.
- Controllable dynamic response to ambient forcing - An important requirement for the current study was to be able to dynamically vary, in a controlled fashion, the hydrodynamic model boundary condition for flow, dilution and effluent concentration. Primarily, this control is required to capture variations in the performance of diffuser in terms of effluent dilution as a result of unsteady ambient current magnitudes as well as outfall discharges.
- Hydrodynamic model grid and time step independence - This is required to ensure that grid and time-step related numerical artefacts are minimised or eliminated entirely, primarily to reduce associated predictive uncertainties. In addition, it is considered important to be able to apply the same methodology to different hydrodynamic models (or model configurations) and facilitate consistency of prediction without needing to retrospectively alter a grid dependent insertion method to suit.

In this study, the same linkage technique presented in Botelho *et al.* (2016) was adopted. This technique addresses the drawbacks of previous approaches, the most significant of which was that constituents with appreciable background ambient concentrations (i.e. salinity), required the implementation of artificial sinks to remove excess constituent mass from the system (e.g. Marti *et al.* 2011, Botelho *et al.* 2013, BMT WBM 2014). Methods applied in this study are free from this limitation.

4.4.7.3 Model integration

Model integration was accomplished by mapping the dilution fields computed by the CFD model according to the velocity field calculated by the farfield model and the PSDP operation. The mass, heat and DO delivered by the discharge in each model time step was then appropriately distributed in the farfield model domain (in three dimensions, not just at the seabed) according to the dilution map. This process is illustrated in Figure 4-10.

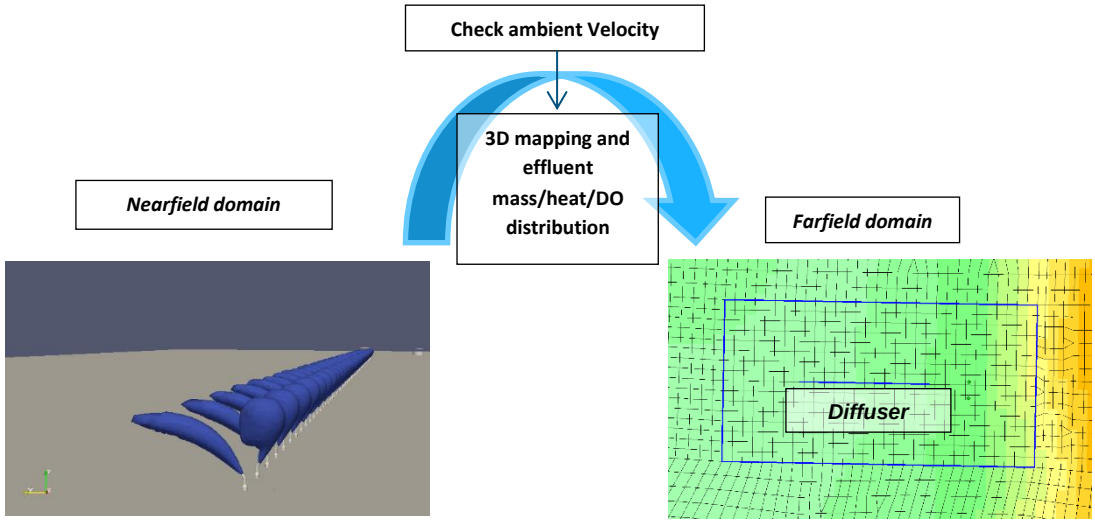

Figure 4-10 Schematic of the translation of the nearfield effluent mass distribution into the farfield Model

The linkage technique presented above has two attractive features:

(1) It provides a realistic three-dimensional depiction (map) of the plume shape (provided there is sufficient resolution) in the farfield model. This is a major difference from Botelho *et al.* (2013), in which a single dilution value (as opposed to a complete three-dimensional field) was tabulated for each velocity percentile; and

(2) The linkage is naturally mass-conservative and the mixing of the discharge with the ambient takes into consideration any existing effluent constituent mass, either previously discharged by the outfall or present as part of the ambient background. As already mentioned, previously adopted linkage techniques required the establishment of artificial sinks to balance background concentrations (e.g. Marti *et al.* 2011, Botelho *et al.* 2013) and the assumed dilutions did not account for mixing with brine discharged in previous time steps.

4.4.7.4 Salinity, temperature and DO

The salinity, temperature and DO for the discharge before distribution using the linkage technique are presented in Table 4-2.

Table 4-2 PSDP boundary specification

Variable	Specified value
Flow Rate (m^3/s)	2.5
Temperature	Intake + 2.5 ^oC
Salinity	61.4
DO	100% saturation

4.4.8 Intakes and other discharges

Intakes and outfalls related to other industries operating in Cockburn Sound were included in the model. Whilst detailed (or anything other than typical or average) data describing the discharges for the simulation periods undertaken in this study were not available, these inputs were collated from

local industry reports where and if possible, are summarised in Table 4-3, and mapped in Figure 4-3. In particular, it is noted that the different simulated periods saw a change in the number, quantity and quality (i.e. flow, temperature, etc.) of the discharges and intakes associated with the Kwinana Power Station and the Newgen Kwinana Gas Fired Power Station. A 100% DO saturation (based on temperature and salinity, Riley and Skirrow 1974) was assumed for the boundary conditions.

Given the focus on the impacts of the PSDP discharge and the limited (poor) information available for the other intakes and discharges, separate nearfield modelling was not undertaken (or justifiable) for any of these additional industrial discharges.

Table 4-3 Industrial discharges and intakes boundary conditions

Simulation Period	Boundary condition	Intake	Outfall	Flow rate (m^3/s)	Temperature (°C)	Salinity (-)	DO	SOurce
Winter - Spring 2006 Summer - Autumn 2007 Suumer - Autumn 2008 Winter - Spring 2008	Kwinana Power Station Stage A and B	Intake A/B	Canal A/B	9.2	Ambient + 9	Ambient	100% saturation at Discharge	CWR (2009)
	Cockburn Power Station and Kwinana Power Station Stage C	Intake C	Canal C	9.82	Ambient + 9	Ambient		
February to April 2011	Kwinana Power Station Stage A	Intake A/B	Canal A/B	4.6	Ambient + 9	Ambient	100% saturation at Discharge	CWR (2009)
	Newgen Kwinana Gas Fired Power Station	Intake C	Newgen Outfall	5.0	Ambient + 9.5	Ambient		Newgen (2014)
	Cockburn Power Station and Kwinana Power Station Stage C	Intake C	Canal C	9.82 (Feb-Mar) 4.74 (April)	Ambient + 9	Ambient		CWR (2009) and additional information from URS (2011) – Appendix G
February to April 2013	Kwinana Power Station Gas Fired	Intake A/B	Canal A/B	3.0	Ambient + 3.5	Ambient	100% saturation at Discharge	Flows from URS (2014) Table 3 Appendix F – Max Jan to Apr 2014 Temperature increase from average 2016-2017 data provided by Synergy
	Newgen Kwinana Gas Fired Power Station	Intake C	Newgen Outfall	5.0	Ambient + 9.5	Ambient		Newgen (2014)
	Cockburn Power Station and Kwinana Power Station Stage C	Intake C	Canal C	9.82	Ambient + 9	Ambient		CWR (2009)
October - November 2015	Kwinana Power Station Gas Fired	Intake A/B	Canal A/B	2.6	Ambient + 9	Ambient	100% saturation at Discharge	Flows from URS (2014) Table 3 Appendix F – Max Jan to Apr 2014 Temperature increase from average 2016-2017 data provided by Synergy
	Newgen Kwinana Gas Fired Power Station	Intake C	Newgen Outfall	5.0	Ambient + 9.5	Ambient		Newgen (2014))
	Cockburn Power Station	Intake C	Canal C	4.74	Ambient + 9	Ambient		CWR (2009)
All periods	PSDP	PSDP Intake	See Section 4.4.7	4.23	See Section 4.4.7	See Section 4.4.7	100% saturation at Discharge	Section 4.4.7
	BP Refinery	BP Intake	BP outfall	5.4	Ambient + 13.83	Ambient – 0.38		CWR (2009)
	Tiwest	No Intake	TiWest Outfall	0.125	Ambient +3	24		
Note: All outfall flows equal intake flows unless otherwise noted								

4.5 Turbulence closure scheme

The General Ocean Turbulence Model (GOTM) was coupled with the 3D TUFLOW FV hydrodynamic model in order to simulate the vertical mixing processes in the presence of density stratification (http://www.gotm.net/).

4.6 Hydrodynamic model parameterisation

The hydrodynamic model calibration was undertaken in 3D baroclinic mode adopting a hybrid sigma/z-coordinate layer scheme. This scheme comprised 53 layers with the following vertical thicknesses:

- -3.0 to -22.0 mAHD (38 layers): 0.5 m
- the remaining layers thicknesses were respectively 1.0 m, 2.0 m, 5.0 m, 10.0 m, 10.0 m, 25.0m, 25.0 m, 50.0 m, 50.0 m, 300 m, 500 m, 500 m, 500 m, and 3000 m. Between the water surface and -3.0 mAHD, 4 sigma-layers (i.e. varying in thickness with the surface elevation) were applied and were able to vary in their thicknesses depending on the water surface elevation changes.

Salinity and temperature were included within the model as density-coupled scalar constituents, thus supporting simulation of baroclinic density gradient forcing and the effect of vertical density stratification on turbulent mixing in the water column.

The TUFLOW FV model configurations and parameterisations are summarised in Table 4-4.

Table 4-4 Summary of TUFLOW FV model configuration and parameterisations

Model configuration description	Model/Value
Horizontal momentum mixing model	Smagorinsky
Horizontal scalar mixing model	Smagorinsky
Bottom drag model	Derived from application of the “log-law”
Horizontal spatial order	Second order
Vertical discretisation	Hybrid sigma/z
Vertical spatial order	Second order
Bottom roughness length scale	0.02 m
Vertical mixing model	2-equation κ-ω with default parameters (GOTM library)

5 Model simulations

Several simulations were undertaken to demonstrate that the models described in Sections 3 and 4 are fit for purpose. Calibration and validation included comparisons against:

- Department of Transport water level data at Mangles Bay (Figure 2-4). The supporting simulations were correspondingly undertaken for the periods of May to July 2006, February to March of 2007, January to March of 2008, August to September 2008, and March 2011.
- FPA water level data at Stirling Channel Beacon A. The supporting simulations were correspondingly undertaken for the periods of April 2013 and October to November 2015.
- FPA water velocity data at the Northern Basin and Spoil Ground stations (Figure 2-4). The supporting simulations were correspondingly undertaken for the periods of May to July 2006 and February to March of 2007. Therefore, the May to July 2006 simulation did not include the PSDP discharge.
- Water Corporation water quality data (temperature, salinity and DO) at the North Buoy, Central Buoy and South Buoy stations (Figure 2-4). Both continuous data (termed RTMS) and profile data were used for comparisons. Supporting simulations were undertaken for the periods of January to March of 2008, August to September 2008, March 2011 and April 2013. All these simulations included the PSDP discharge. For the 2011 and 2013 simulations data at North Buoy was not available (i.e. RTMS) or very limited (i.e. a single profile) and therefore was not used for comparisons.
- Water Corporation water quality profile data (temperature, salinity and DO) at Callista Channel and its surroundings into Cockburn Sound's deep basin (Figure 2-16) collected as part of the MMMP. Supporting simulations were undertaken for the periods of the events in March 2011 and February to April 2013.
- Salinity measurements undertaken by CWR (2007) that tracked the brine plume in the immediate surrounds of the PSDP diffuser. These comparisons were necessarily qualitative in nature as the raw data was not available to this study.
- Evaporation rates.

Initial conditions for temperature and salinity were provided by HYCOM + NCODA data, and DO concentrations were assumed to be 95% of saturation based on the temperature and salinity fields. Model outputs were extracted every 15 minutes.

The simulations of the periods May to July 2006 and February to March of 2007 were specifically undertaken for comparisons with velocity, given it was the only period with measurements available. For scalars (temperature, salinity and DO) focus was given to the transition between summer and autumn periods (January to March of 2008, March 2011 and April 2013) when dissolved oxygen concentrations often reduce in response to stratification. This is also partly because more data were available over those periods as a result of the additional monitoring undertaken when conditions deteriorated. The simulation for the August to September 2008 period was undertaken to show the model's ability to replicate winter dynamics under the influence of Swan River flows. Finally, although no scalar or velocity data exists for comparisons over October to November 2015, the period was

chosen as it encompasses a fish kill event in Cockburn Sound (Department of Fisheries 2016, Pattiaratchi 2016).

5.1 Water level comparisons

5.1.1 Measurement specifications

Water level data were available from:

- Department of Transport at Mangles Bay between August 2003 and November 2011; and
- FPA at Stirling Channel Beacon A between July 2011 and November 2016.

Both data sets were available at every 5 minutes and were referenced to Fremantle Low Water Mark (-0.76 mAHD).

5.1.2 Model Comparisons

For each of the modelled periods, visual comparisons were made between model and measured water levels. Additionally, a harmonic analysis using the software t_tide (Pawlowicz et al. 2002) was undertaken to separate astronomical tides from the total water elevation signal. Visual comparisons between the astronomical tides and the residuals (i.e. the difference between the total and the astronomical tides) were also undertaken.

The model predictive skill was also tested statistically with calculations of the Index of Agreement (IOA), Mean Absolute Error (MAE), and Root Mean Square Error (RMSE) as defined in Appendix D. At project inception, the following calibration targets were agreed as indicators of satisfactory model validation (Table 5-1):

Table 5-1 Calibration goals for water levels

Variable	IOA (-)	MAE (m)	RMSE (m)
Water Level	≥ 0.8	≤ 0.10	≤ 0.15

Time series comparisons between measured and modelled water levels are presented for each of the simulation periods in Figure 5-1 to Figure 5-6.

It is noted that the gauge did not consistently record between approximately 15 and 30 May 2006, and that there was a phase mismatch between model and field data (Figure 5-1). As the gauge seemed to be presenting some problems, the comparisons for that period need to be interpreted with caution. Nevertheless, the data over that period were still included in all error calculations. Removing these likely faulty data would improve model calibration statistics.

Overall both tidal harmonics and residuals show good agreement between model and field data. As can be seen in comparison of residuals, the model residual captured sub-tidal oscillations well.

In winter and spring (Figure 5-1, Figure 5-4, and Figure 5-6), the sub tidal frequencies are generally influenced by the passage of low- and high-pressure systems rather than the propagation of CSWs (Section 2.2.2), noting no Tropical Cyclones were identified over these simulation periods. For the summer to autumn periods (Figure 5-2, Figure 5-3, Figure 5-4, and Figure 5-5), the potential

signature of CSWs appears as sub-tidal oscillations. It is noted that the majority of simulated periods in summer and autumn coincided with the formation of tropical cyclones in the northwest of Australia: January to March 2007 (TC Humba, TC George, TC Jacob and TC Kara), February and March 2008 (TC Nicholas and TC Ophelia), March 2011 (TC Carlos), and April 2013 (TC Victoria).

The IOA, MAE and RMSE (Table 5-2) were consistent across all simulated periods and within the calibration targets proposed in Table 5-1. The statistics show the model has an adequate performance for the simulation of Cockburn Sound.

Model simulations

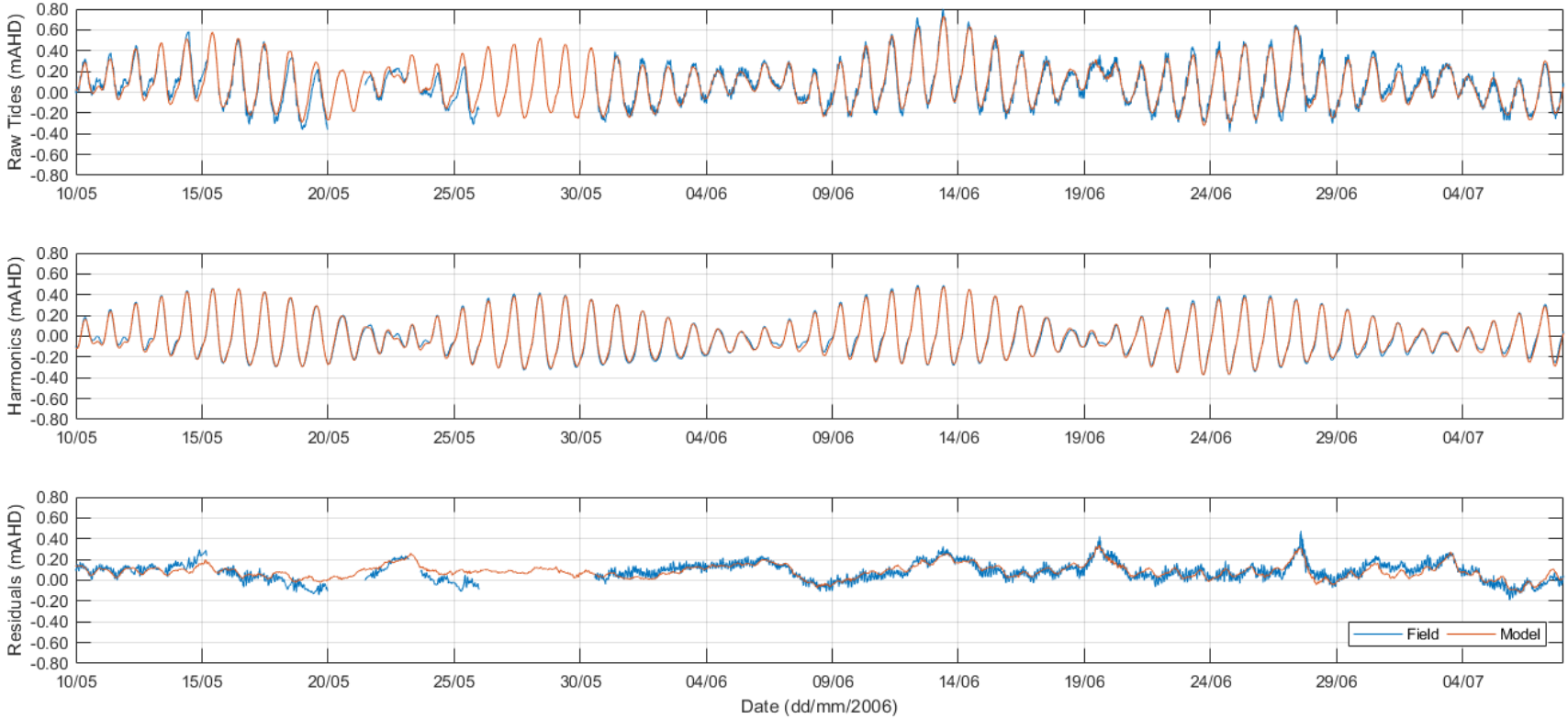

Figure 5-1 Comparison between measured and simulated water levels at Mangles Bay for May to July 2006

Model simulations

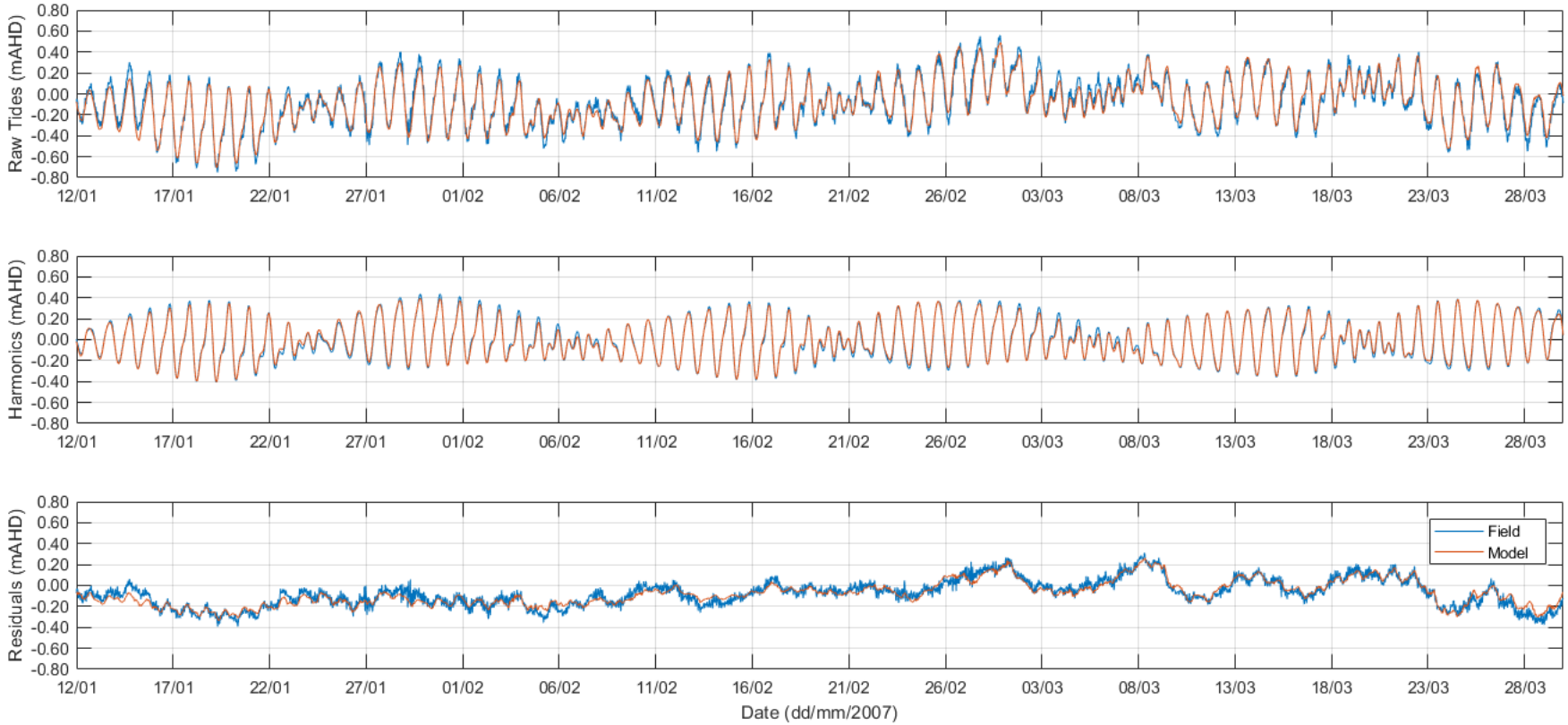

Figure 5-2 Comparison between measured and simulated water levels at Mangles Bay for January to March 2007

Model simulations

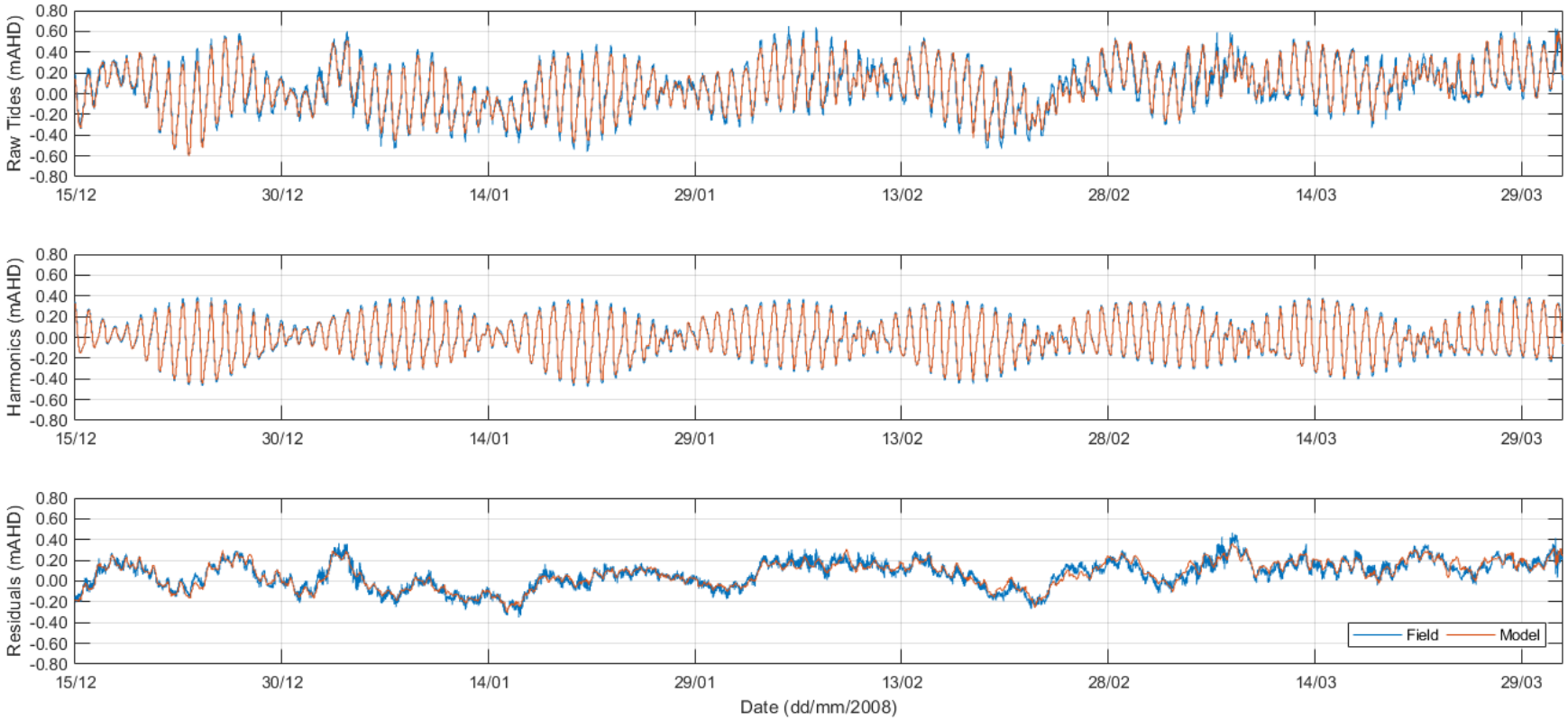

Figure 5-3 Comparison between measured and simulated water levels at Mangles Bay for January to April 2008

Model simulations

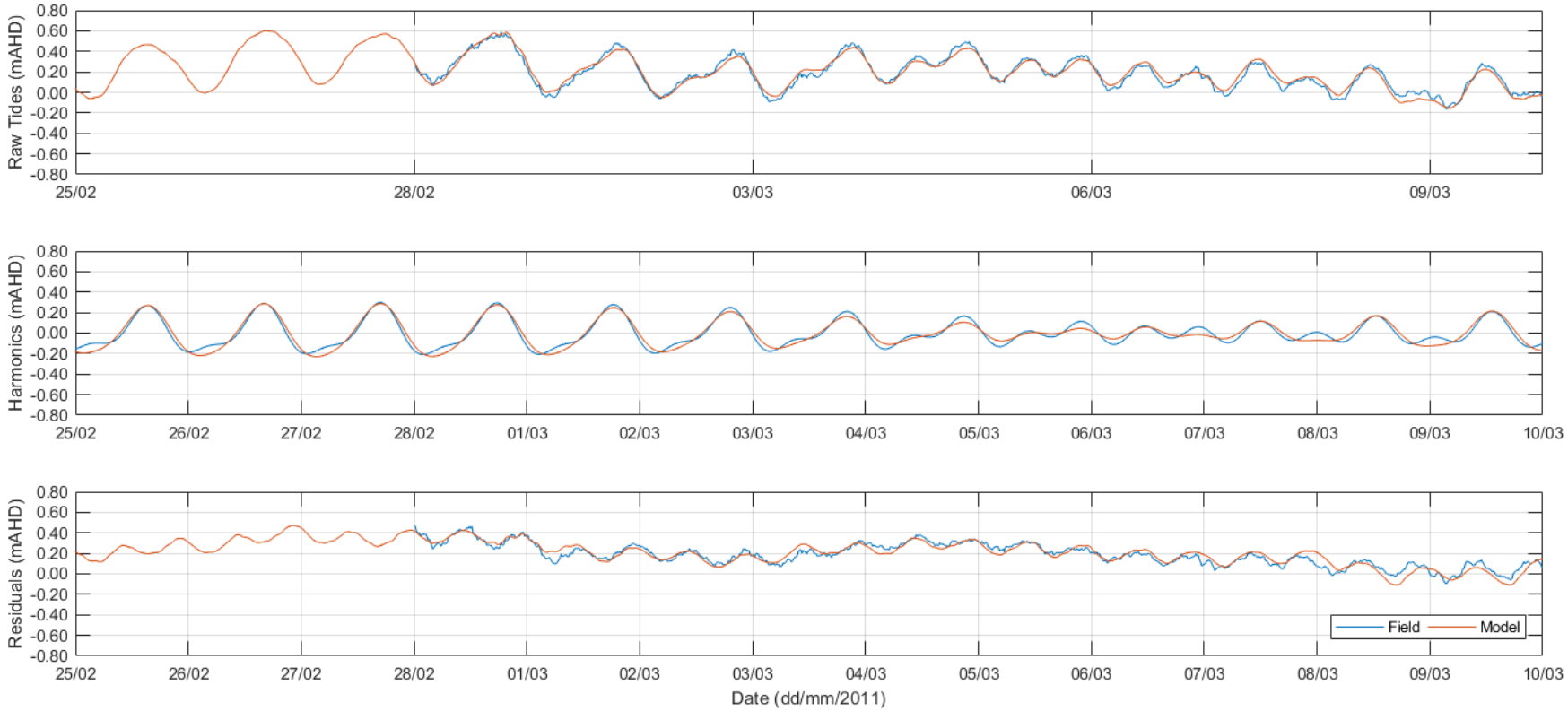

Figure 5-4 Comparison between measured and simulated water levels at Mangles Bay for March 2011

Model simulations

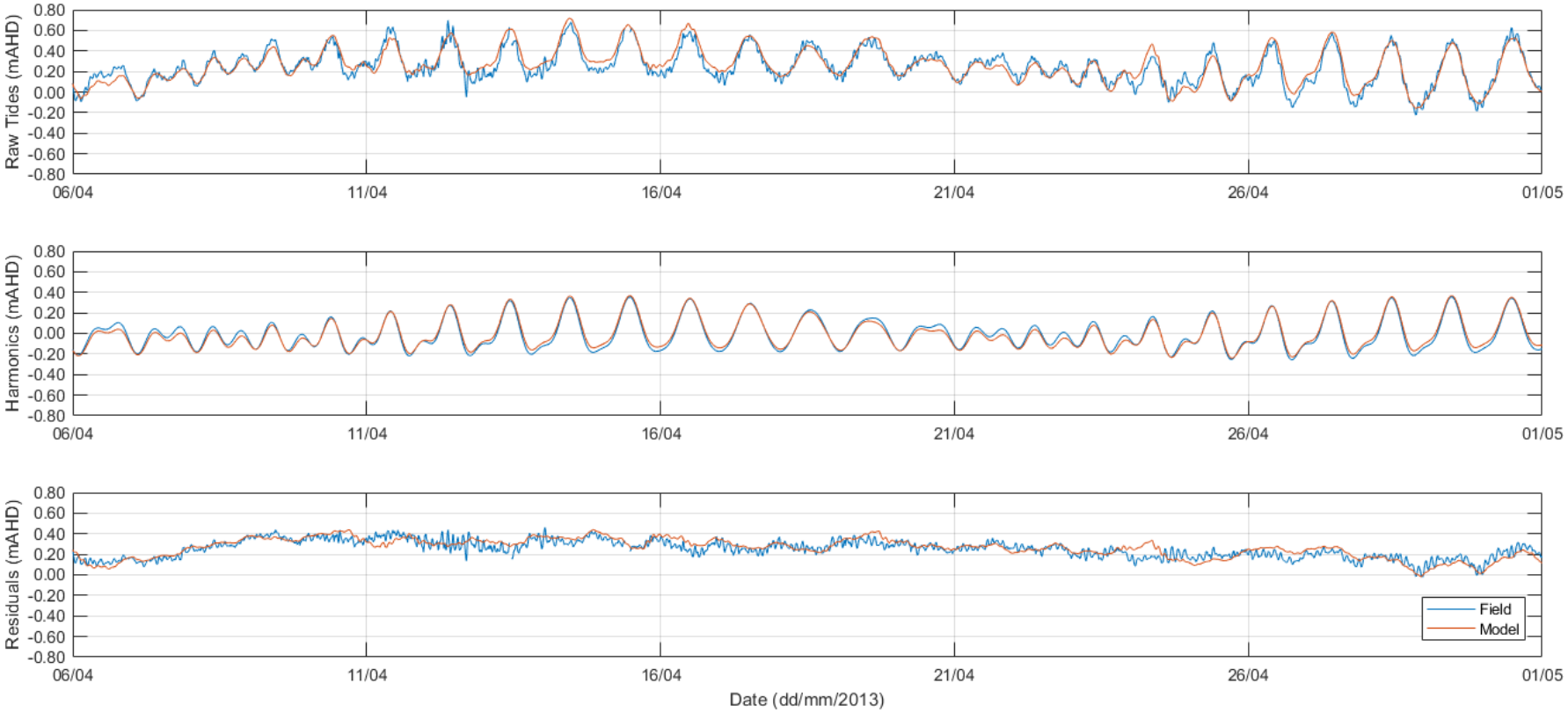

Figure 5-5 Comparison between measured and simulated water levels at Stirling Channel Beacon 5 for April 2013

Model simulations

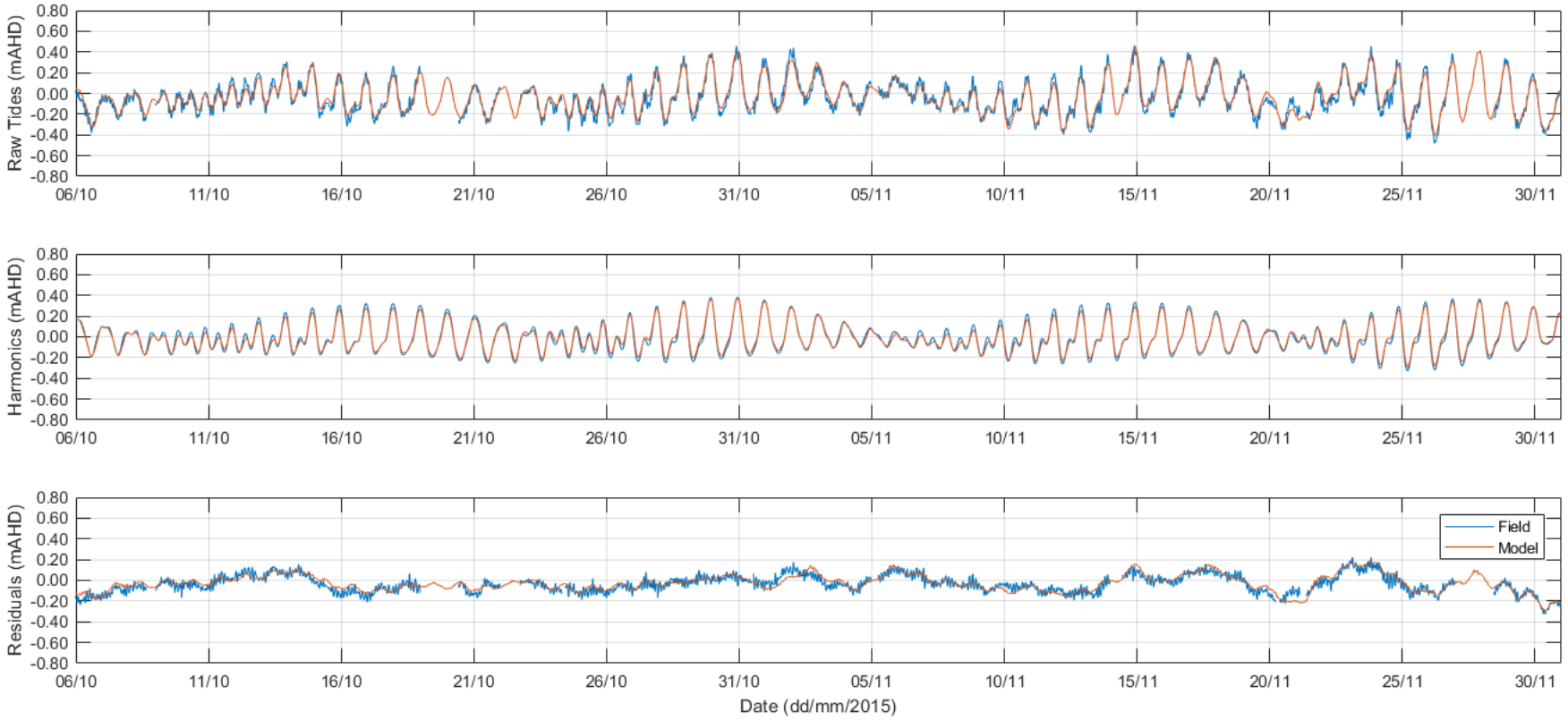

Figure 5-6 Comparison between measured and simulated water levels at Stirling Channel Beacon 5 for October to November 2015

Table 5-2 Error measures for water levels

Period	Location	IOA	MAE (m)	RMSE (m)
May to July 2006	Mangles Bay	0.983	0.040	0.051
January to March 2007		0.987	0.039	0.048
January to April 2008		0.986	0.038	0.053
July to October 2008		0.988	0.037	0.046
March 2011		0.984	0.033	0.039
April 2013	Stirling Channel Beacon 5	0.968	0.049	0.060
October to November 2015		0.979	0.036	0.045
Calibration goals		≥ 0.8	≤ 0.10	≤ 0.15

5.2 Velocity comparisons

5.2.1 Measurement specifications

Acoustic Doppler Current Profiler (ADCP) velocity measurements were collected in winter 2006 and summer 2007 at two locations for each campaign (the locations of the instruments are presented in Figure 2-4). Station *Spoil Grounds* was located within the eastern shore area at a depth of approximately 6.5 m. Station *Northern Basin* was located in the deep basin at approximately 19.0 m depth. Details of the ADCP arrangements are summarised in Table 5-3.

Table 5-3 Details of ADCP arrangements

Station	Deployment depth	Number of bins	Bin heights	Bin spacing	Sampling Interval
Spoil Grounds	6.0 m	8 (winter) 9 (summer)	1.6 m to 5.1 (winter) 1.6 m to 5.6 (summer)	0.5 m	10 minutes
Northern Basin	18.5 m	14 (winter) 15 (summer)	2.5 m to 15.5 (winter) 2.5 m to 16.5 (summer)	1.0 m	10 minutes

The winter deployment was undertaken between 10 May and 07 July 2006, whilst the summer deployment was undertaken between 31 January and 29 March 2007.

5.2.2 Model comparisons

5.2.2.1 May to July 2006

Comparisons between simulated velocities and ADCP measurements in the transition from autumn to winter (May to July 2006) at Spoil Grounds and Northern Basin are shown in Figure 5-7 to Figure 5-12, respectively. The comparisons in Figure 5-7 and Figure 5-11 are shown in terms of velocity components colour contours, where the colours indicate either of the velocity components (E-W being east-west component, with negative values being water directed west and analogously N-S being north-south component, with negative values being water travelling south), as given by the respective colour bars. The x- and y-axes show time and height above the seabed, respectively. The same comparison figures are shown over shorter time intervals (i.e. with higher temporal resolution)

in Appendix E. Time series of velocity components at different ADCP bins near the surface (Figure 5-8 and Figure 5-12), mid water column (Figure 5-9 and Figure 5-13) and near the bed (Figure 5-10 and Figure 5-14) are also presented for comparisons and shown over shorter intervals in Appendix E.

The contours shown in Figure 5-7 and Figure 5-11 demonstrate that the model reproduced key characteristics of the velocity field at the different stations. For example, at Spoil Grounds, observed and simulated E-W velocities were generally weaker than N-S velocities. In addition, vertical shear of the E-W component was more prominent than for the N-S component. The velocity components were generally lower than 0.05 m/s with episodic northerly winds driving increased velocity magnitudes up to 0.15 m/s every 7 to 10 days. The model captured these transitions to southerly flows during the wind events, as well as the velocity increases throughout the water column. This points to the model's ability to respond appropriately to wind driving and also to reproduce vertical momentum exchange at Spoil Grounds.

At Northern Basin, and in contrast with Spoil grounds, both measured and simulated velocities presented a three-layered structure at times, with surface and bottom velocities exceeding those at mid depth. This structure was more evident with the passage of cold fronts when winds shifted from the north and the northwest to southwest. Under these occasions, velocity components in the surface and bottom layers were up to 0.15 m/s (see Section 2.2.2.1).

The model reproduced some of these events well (i.e. 28 to 30 May, 20 to 21 June, and 27 to 28 June – see e.g. Figure 5-15; also Appendix E). However, in a similar event on 15 May, the model showed a stronger tendency to move water in the northerly direction, whilst field measurements indicated velocities moving in more of a south-easterly direction (Figure 5-16; also Appendix E). This indicates that, for that particular event, the model was more responsive to an increase in the N-S component of the wind direction, whilst the field data indicated a stronger response to the wind moving in the easterly direction.

It was evident in both field data and model results that the deep basin of the Sound is subject to internal motions (i.e. internal waves), and these are also influenced by the Earth's rotation (see e.g. D'Adamo 2002). The response to a wind event will depend on the phase and amplitude of these internal motions. As a result, model agreement in terms of velocities will depend on correspondence of the internal motion phase prior to an event start. This may explain why a similar event was better reproduced on 28 May (Figure 5-15) than on 15 May (Figure 5-15). BMT is not aware of studies that have specifically considered internal wave activity in Cockburn Sound.

On the other hand, the water motion in the shallow areas (i.e. Spoil Grounds) was not layered, so that correspondence with the internal motions was less impactful on model performance.

The model predictive skill was also tested statistically with calculations of the Index of Agreement (IOA), Mean Absolute Error (MAE), and Root Mean Square Error (RMSE) as defined in Appendix D. At project inception, the following calibration targets were agreed as indicators of satisfactory model validation (Table 5-4):

Table 5-4 Calibration goals for velocity

Variable	IOA (-)	MAE (m/s)	RMSE (m/s)
X-component Velocity	≥ 0.5	≤ 0.05	≤ 0.06
Y-component Velocity	≥ 0.5	≤ 0.05	≤ 0.06

This statistical evaluation of the predicted currents at the ADCP locations during the May to July 2006 period is provided in Table 5-5 and Table 5-6 for Spoil Grounds and Northern Basin, respectively. These statistics confirm the model's predictive ability with velocity IOA's generally above 0.5 (only a few instances with lower values that coincided with the regions of low current velocities, i.e., large noise to signal ratio in measurements). MAE was between 0.02 and 0.03 m/s for Spoil Grounds and between 0.02 and 0.04 m/s for Northern Basin. RMSE was between 0.02 and 0.03 m/s for Spoil Grounds and 0.03 and 0.05 m/s for Northern Basin. These results are similar to other modelling investigations compared to the same data set (CWR 2009) and within the model ranges agreed at project inception (Table 5-4).